PHASE RELATIONS AND Pt SOLUBILITY IN SULPHIDE MELT IN THE FE-NI-CU-S SYSTEM AT 1 ATM: IMPLICATIONS FOR EVOLUTION OF SULPHIDE MAGMA IN THE MERENSKY REEF, BUSHVELD COMPLEX, SOUTH AFRICA.

by

Luhann Marlon Theron

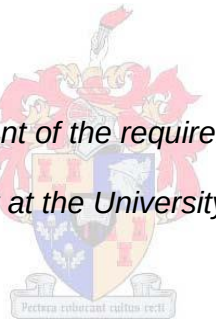

Thesis presented in partial fulfilment of the requirements for the degree Masters of science in Geology at the University of Stellenbosch

Supervisor: **Professor. Gary Stevens**

Faculty of Science

Department of Earth Sciences

March 2O13

***

Declaration

By submitting this thesis/dissertation, I declare that the entirety of the work contained therein is my own, original work, that I am the sole author thereof (save to the extent explicitly otherwise stated), that reproduction and publication thereof by Stellenbosch University will not infringe any third party rights and that I have not previously in its entirety or in part submitted it for obtaining any qualification.

Signature:

Date: December 2012

Dedication

I dedicate this dissertation to my family, especially…

my mother, for her positive and endless support.

my two older brothers for showing me the way and paving the road to success for me.

and my father for opening my eyes to the world. You have vision, serenity and unbounded wisdom.

My parents instilled the importance of hard work

and higher education in my life

and all my success is ingrained in their dreams.

My only wish for the above-mentioned individuals is

for them to be as proud of me as I of them.

Lastly, I want to dedicate this dissertation to the one who gave me the talents and abilities.

I pray that my life is a testimony to Your greatness.

Prologue

This dissertation is compiled in the following manner. The intention of the author was to present his research in the form of a scientific paper, prepared for submission to a professional journal of international standard. Therefore the majority of this dissertation is compiled in this format. To comply with the technical aspects set forward by the academic institution (University of Stellenbosch), the scientific paper is preceded by this prologue, an introductory chapter and an abstract (in two languages). Formatting, line spacing etc., of the scientific paper is also not done in the format of any specific academic journal, but was adjusted to fit the guidelines outlined by the academic institution, while trying to imitate the look and feel of a scientific paper.

The introductory chapter serves to introduce the reader to the research background, research area and other work relevant to the research subject. It also expands on the research methodology including experimental design and analysis. The reader will notice that some of this information will be mentioned and discussed in the paper format of the dissertation as well. The introductory section ends with a statement of the research goals and possible outcomes.

All the experiments reported within the scientific article were conducted within the experimental lab at the Department of Earth Sciences and the Department of Chemical Engineering, University of Stellenbosch. The author was responsible for developing his own experimental techniques, lead by research from literature and assistance from his colleagues. Starting material and the standards for LA-SF-ICP-MS analysis was generated in-house as well and the methodology for this is stipulated in later chapters.

Abstract

It is widely accepted that sulphide is the carrier and concentrator of PGEs during magmatic mineralization episodes in the Merensky Reef (MR). PGE concentration peaks and sulphide volume percent peaks are very closely correlated. Koegelenberg, (2011), showed in an experimental investigation that sulphide movement through a cumulate silicate and cumulate oxide pile behave in such a way that sulphide melt gets trapped in chromitite layers. When looking at the compositional distribution of sulphide within the MR it is noted that not only does the sulphide volume percent varies with MR stratigraphy but also the sulphide composition. Sulphide composition is more Cu-rich in the chromitite layers and more Fe and Ni dominated in the hanging wall to the chromitite layers. Until now the more Cu-rich assemblage of the chromitite layers are accepted to be of a sulphide melt composition compared to the Fe and Ni dominated Monosulphide Solid Solution or MSS composition in the hanging wall. In this study we used an experimental approach with a sulphide starting composition thought to exist as the parental sulphide composition of the MR to investigate the phase relations with changing temperature. It is found that the sulphide composition in the chromitite layers represent a sulphide melt composition at 1000 ± 50ºC. At 1000ºC, 50% of the sulphide system would exist as a melt. This Cu-rich melt would have segregated from the MSS and be trapped in the chromitite layer. Also at 1000ºC the partitioning of the Pt would have induced a secondary enrichment step of the Pt concentration in melt through the partitioning of Pt between a sulphide melt and a sulphide solid phase.

The experimental evidence in this study points towards a possible source for the parental sulphide magma to the MR, which could have been a slightly Cu enriched mantle sulphide composition. Also, the secondary enrichment of Pt through sulphide melt fractionation at 1000ºC plays an important role in the shaping of the ore body.

Opsomming

Dit word wydliks aanvaar dat die sulfied fraksie van die Merensky Rif (MR) die draer en die konsentrasie agent is vir Platinum Groep Elemente (PGE`s) gedurende mineralisasie episodes. PGE konsentrasie en sulfied volume persentasie is op `n hoogtepunt by gelyke stratigrafiese posisies in the MR. Koegelenberg, (2011), het deur middel van eksperimente bewys dat `n sulfied smelt deur `n voorafbestaande kumulaat laag kan beweeg en dat veranderende fisiese eienskappe tussen sulfied smelt en silikaat kristal en sulfied smelt en chromiet kristal, die sulfied smelt sal opsuig en verhoud om verder deur te suipel. Dit is egter oplettend dat nie net die sulfied volume persentasie varieer as `n funksie van die MR stratigrafie nie, maar ook die sulfied samestelling. Die meer Cu-ryke sulfied samestelling in die chromiet lae word aanvaar as `n sulfied smelt fraksie en die meer Fe en Ni dominerende sulfied samestelling in die oorhangende wandgesteentes verteenwoordig die Monosulfied Vaste Oplossing (MVO) soliede fase. In hierdie studie maak ons gebruik van eksperimentele petrologie tesame met `n begin samestelling verteenwoordigend van die oorsprong sulfied samestelling van die MR, om die fase verwantskappe van hierdie spesifieke samestelling te ondersoek. Dit word gevind dat die fraksionering tydens die vorming van die MR plaasgevind het by ongeveer 1000 ±50 C. By hierdie temperatuur is 50% van die sisteem teenwoordig as `n smelt fase. Hierdie Cu-verykte smelt was daartoe instaat om deur die silikaat laag te suipel, geskei te raak van die Fe en Ni dominerende MVO en vasgevang te word in die chromiet lae. Hierdie fraksionering van die sulfied smelt het ook `n sekondêre effek gehad op die verspreiding van Pt tussen sulfied smelt en sulfied soliede fases.

Hierdie eksperimentele bewyse dui eerstens op die moontlikheid van `n sulfied smelt in die MR wat sy oorsprong vanuit `n effense Cu-verykte mantel bron kan hê, en tweedens op

die belangrikheid van `n sekondêre proses vir Pt re-distribusie tydens die vorming van die MR.

Acknowledgements

There are so many individuals to acknowledge in the completion of this dissertation. I would like to start with the National Research Foundation of South Africa for supporting the study via SARChI funding to Prof. Gary Stevens. Support from ANGLO Platinum is also gratefully acknowledged. Prof. Gary Stevens took me straight from undergrad into the Centre for Crustal Petrology. Thank you for organizing all of the logistics around financing. Never was there a day where I had to worry about money.

To my colleagues Prof. Gary Stevens and Cornè Koegelenberg in the assistance in the experimental lab, I would like to extend a great deal of acknowledgement to your guidance. We have found the figuratively 1999 ways how to: “not make a light bulb.”

To the analytical staff from the Centre for Analytical Facilities; Madelein Frazenburg on the Scanning Electron Microscope and Dirk Frei at Laser Ablation. Analyses on sulphide materials were as new to you as to me. Acknowledgement for your dedication and support in data capturing and re-working.

For the writing up of the final compilation I would like to extend acknowledgement to my supervisor, Prof. Gary Stevens. Your contribution and guidance gave sense to the data and the way it is presented.

Table of content:

List of Figures

List of Tables

1. General introduction

Study area

The Bushveld Complex (BC) is situated in the northern parts of South Africa in the provinces of North-West, Limpopo and Mpumalanga. The complex extends 450 km east-west and 350 km north-south, making it the largest of its kind in the world with an aerial extend of ~65 000 km_2 (Eales & Cawthorn, 1996), an area size the same as Ireland. The largest part of the complex is however covered with younger deposits and the mafic part of the complex (the Rustenburg layered suite; RLS), outcrops in three identifiable lobes known as; 1) the western lobe which forms an arc from Pretoria to Rustenburg to Bela-Bela, 2) the eastern lobe extending from North of Belfast to Burgersfort and 3) the northern lobe from Potgietersrus (Mokopane) to Villa Nora. Comprehensive studies on BC outcrop maps, stratigraphy and lithology are widespread in literature. Some examples of the best summaries can be found in Kruger, (1994), Viljoen, (1999), Naldrett, (2004), Smith, et al., (2004), Van der Merwe, (2008), Cawthorn, et al., (2002) and Scoates & Friedman, (2008). Below follows a summary of the different rock types and their stratigraphic positions, as a more complete description including intrusion conditions and tectonic setting would be repetitive and superfluous to this study.

Lithologies vary from ultramafic igneous rock types such as peridotite, harzburgite and dunite in the lower sections, to mafic norite and gabbro in the middle sections, to the more felsic intrusives near the top known as the Lebowa granite suite. Stratigraphically the BC can be divided into four distinctive suites of igneous rocks (after Naldrett, et al., 2009) namely; 1) the early pre- and later syn-RLS mafic sills, 2) the Rooiberg felsites, 3) the Rustenburg layered suite (RLS) and 4) the Lebowa granite suite. The layered sequences of the BC which is responsible for the BC distinction as layered intrusion are restricted to the RLS. In turn the RLS can be divided into five zones (Figure. 1). The Marginal zone (up to 800m thick) consists of norite and minor pyroxenite. The Lower zone (up to 500m thick)

is made up of ultramafic rocks such as bronzinite, harzburgite and dunite (Van der Merwe, 2008). The base of the Critical zone (up to 1.2 km thick) is marked by the appearance of cumulus chromitite (Naldrett, et al., 2009). Petrologists have divided the Critical zone into two parts (Cawthorn, 1999a), 1) the Lower Critical zone (LCZ) which composes bronzinite and chromitites and 2) the Upper Critical zone (UCZ) marked by the appearance of cumulus plagioclase. The Critical zone is overlain by the Main zone (up to 3km thick), which consist primarily of gabbronorites. The uppermost rock units of the RLS known as the Upper zone (up to 2,8km thick), consists of ferrogabbros and gabbronorites (Von Gruenewaldt, 1973)

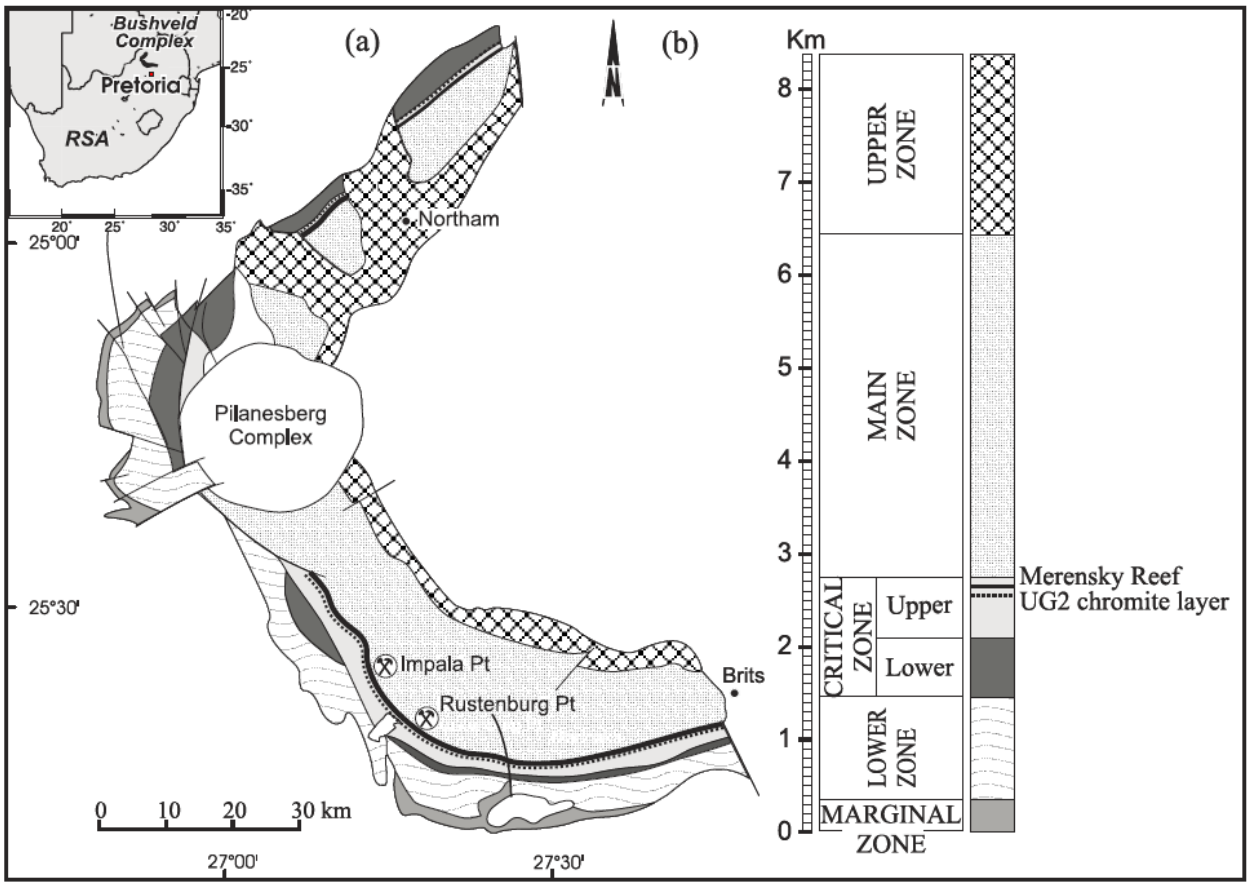

Figure 1: Simplified map and stratigraphy of the western lobe of the RLS. Taken from Godel, et al., (2006), modified after Von Gruenewaldt, 1986 and Eales & Cawthorn, (1996).

The Merensky reef (MR).

Present calculations, as described by Cawthorn, (1999b), indicate about 204 million ounces of proven and probable reserves of Pt contained within the BC up to a depth of 2km. Most of which is concentrated in three main stratigraphic horizons called the UG2 and Merensky reefs and the Plat reef. The MR is stratigraphically situated at the boundary between the upper critical zone and the main zone. The interpretations of this research will be utilized and applied to normal A-type MR as described by Leeb-du Toit, (1986); Barnes & Maier, (2002); Godel, et al., (2006); Godel, et al., (2007). A more in depth description of the regional variation in the MR can be found in papers such as Naldrett, et al., (2009). In its simplest form the MR consists, in a paleo-vertically upwards direction, of; 1) a medium grained, cumulus, footwall anorthosite (mottled anorthosite in mining terms, ranging in thickness between 1 – 10m). 2) a lower chromitite layer that ranges from 2 to 40mm thick, 3) a varying thickness (0-10m) of coarse grained melanorite (feldspathic pyroxenite in local mining terms); 4) an upper chromitite layer 2-10mm thick with an undulating boundary with the overlain melanorite; 5) an upper 30-225 cm of melanorite.

Mineralization of PGEs in the MR and sulphide concentrations is strikingly focussed on the chromite seams. Figure 2 is a presentation of published research by Godel, et al., (2007), which focussed on the base metal sulphide (BMS), platinum group element (PGE) and platinum group mineral (PGM) distribution in the MR. Godel, et al., (2007) also concluded that the majority (~65-80%) of PGEs in the MR are not found in solid solution with BMS, but essentially as PGMs in close correlation with BMS (either included or located at BMS –silicate or oxide boundaries). This relationship between the sulphide volume and PGE occurrence is the principle observation for constructing models to explain the enrichment of the MR.

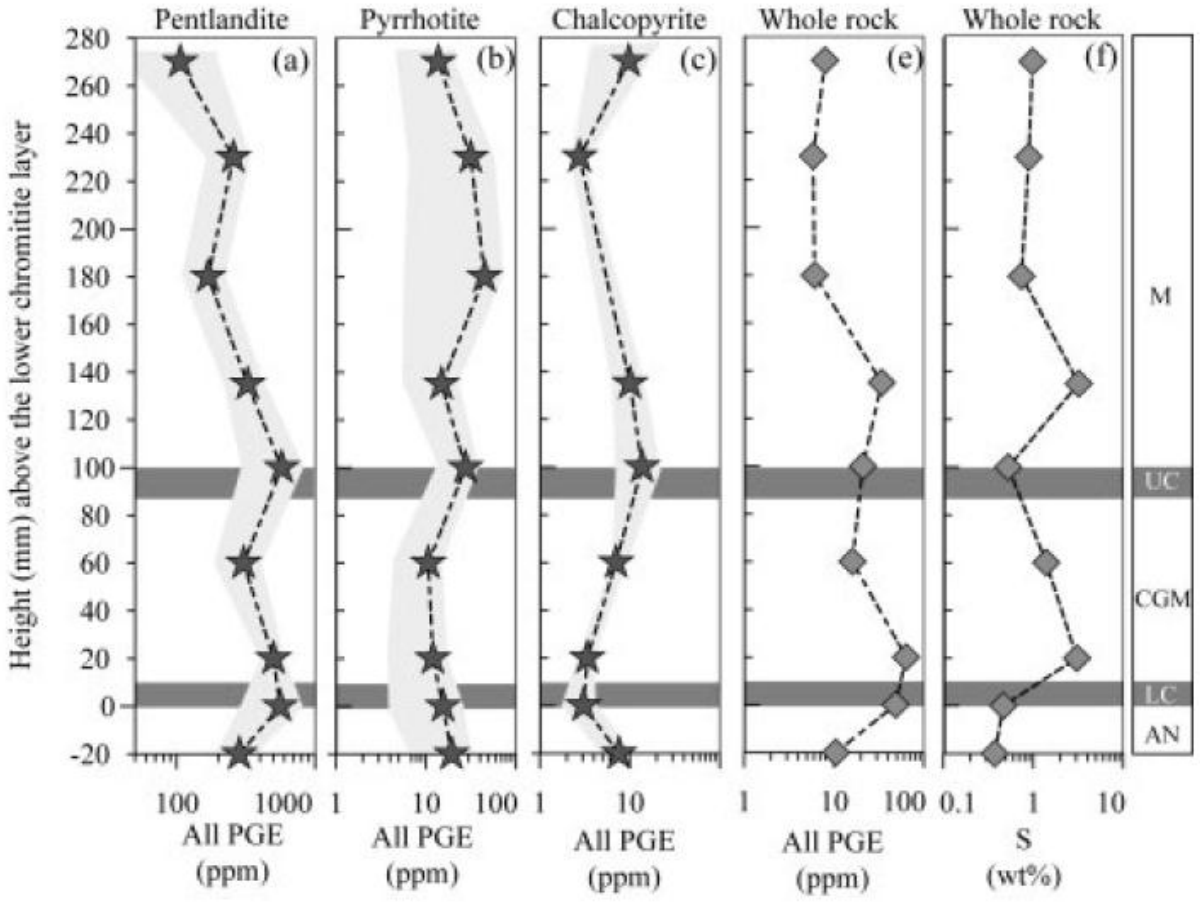

Figure 2: Taken from Godel, et al., (2007). Graphs indicate the close relationship that exists between the sulphide and PGE enrichment at specific stratigraphic positions in the MR. AN = Anorthite, CGM = course grained melanorite.

Mineralization models for the MR.

Models describing processes that resulted in the mineralization of the MR is widely distributed in literature, and most of them illustrate concepts and ideas from different chains of thought. Naldrett, et al., (2009) described two main schools, namely the “uppers” and the “downers”. The ‘Uppers’ school maintains that the metals have been concentrated from the underlying cumulates by ascending, chloride-rich fluids, and have been released at the cumulate-magma interface where accumulating sulphides fixed the metals in situ. The ‘Downers’ consider that the metals were concentrated from above by descending sulphides that concentrated in cumulus rocks close to the cumulate-magma interface. Although in this study the processes of enriching PGEs by an upward migrating fluid is

tacitly assumed, the experimental approach used in this study can by no means test any of the parameters which might distinguish between the two models.

The classic magmatic mineralization model of the MR magmas through the scavenging of PGEs by an immiscible sulphide liquid, first described by Campbell, et al., (1983) and Naldrett, et al., (1986), is still the best accepted model for reef formation. Campbell, et al., (1983) suggested that sulphide immiscibility was the result of the mixing of freshly injected magma with more fractionated magma resident in the magma chamber. Fresh magma influx rose like a plume through the resident magma. Naldrett & von Gruenewaldt, (1989) showed qualitatively how existing sulphur solubility data supported this hypothesis. This model was further supported by the work of Li & Ripley, (2005), which has shown that a wide range in proportions of mixing of the U-type and T-type magma (U-type and T-type magma describe the fresh partially molten mantle melts and the fractionated resident melts, Campbell, et al., 1983, Naldrett & von Gruenewaldt, 1989) can give rise to immiscible sulphide liquid. Other means of sulphide saturation and the formation of an immiscible sulphide liquid were suggested by Cawthorn, (2005). This research suggested that magma mixing might not be required as the established negative effect of an increase in pressure on sulphide solubility (Mavrogenes & O'Neill, 1999) provides the best explanation for both sulphide immiscibility and the formation of the chromitite layers.

One of the biggest concerns with the sulphide associated model is the prediction that the footwall and hanging-wall rocks formed from sulphur saturated magma, and that it ought to have more sulphide (Cu and Ni) than actually observed (Cawthorn, 1999a). Another concern is the communication needed between the sulphide melt and the co-existing silicate melt. With existing knowledge on the element partitioning behaviour between sulphide melt and silicate melt, the MR parental sulphide magma had to interact with an unreasonably high volumes of silicate magma (Cawthorn, 1999a), or PGE partitioning

between the sulphide melt and silicate melt had to be orders of magnitude higher than observed from natural samples (Campbell, et al., 1983). In regards to this, another process was introduced by Tredoux, et al., (1995), called the cluster model. It was suggested that the high partitioning behaviour of PGEs between a sulphide melt and silicate melt might not be required as PGE enrichment in the sulphide melt could be obtained by a mechanical process rather than chemical. Tredoux, et al., (1995) suggested that PGE in a silicate melt do not occur as single atoms or PGE molecules, but would at initial stages of melt formation be present as metallic clusters (50 – 100 atoms). These clusters will then be stabilized by adsorption on to the surfaces of chalcogenides. Important these ligands are not bonded to the clusters by any chemical reactions, but merely adsorbed, and therefore the application of formal partitioning coefficients cannot be applied. These clusters will have a high affinity for a sulphide melt if the system is S-rich and remain in the sulphide melt as inclusions until they can combine and precipitate out as alloys or combine in crystal structure to form PGE-sulphides. In S-deficient systems the clusters will remain in the silicate melt until enough clusters can combine to form alloys. The important implications of this model is the indication that apparent high partitioning coefficients for PGEs between a sulphide and silicate melt needed to concentrate PGE in the MR, can be redundant. If PGEs existed in clusters, the geological system would rather reflect D-values of PGE between metal and silicate, rather than between sulphide- and silicate. The hypothesis set forward by the cluster model however, relies heavily on the experimental information that shows the stability of PGE nuclei or clusters in the silicate melt and also the sulphide melt.

Experimental petrology.

The reason for trying to establish D-values for PGEs experimentally instead of analysing natural samples, is due to the fact that sulphide in natural rocks are not representative of the sulphide stable phases at magmatic temperature. It is well known that at magmatic T conditions (commonly above ~500 ºC) sulphide crystallizes as a monosulphide solid solution (MSS) from a sulphide melt. The low temperature stable phases we observe in natural rocks (pyrrhotite, pentlandite, chalcopyrite, etc.) are the result of exsolution (typically below 400 ºC) from the MSS. Other advantages of experimental petrology includes; 1) the accurate control on parameters such as temperature, pressure and composition, 2) re-productivity of experimental runs and 3) isolated testing of discrete chemical systems.

An introduction to the experimental data available in literature in terms of PGE partition coefficients between sulphide melt and silicate melt and also between sulphide melt and sulphide solid phases can be found in the introductory sections of the second chapter of this dissertation. An explanation of the experimental design and procedures can be found in the experimental design section of the second chapter of this dissertation. In short, this study was set out to conduct a series of experiments in 50 ºC intervals from above the expected liquidus to below the solidus. The principle analytical technique to be used is the scanning electron microscope (SEM) and major element chemistry determined by ED analysis. Chemical composition data was gathered for the stable equilibrium phases at each temperature interval. It was noticed that the quenching of the equilibrium melt had to be dealt with in a very special manner, and an in detail explanation for that can also be found in the second chapter. Detailed imaging was done of both the solid phases and the melt phases.

Reconnaissance sulphide experiments at the University of Stellenbosch.

Reconnaissance experiments done in conjunction with this study are shortly discussed later. This chapter serves as back ground to this work as the results are still in review. The preliminary results presented here are essential to certain aspects of MR mineralization discussed in the discussion and conclusion chapters of this dissertation. The following data was compiled from the dissertation of Koegelenberg C., (2011) and his presentation at the 2012 Igneous and Metamorphic Study Group meeting at the University of the Witwatersrand, Johannesburg.

Chromite-sulphide melt interaction was investigated by allowing sulphide melt, at 1050°C - 900°C and 4kbar, to move downwards through two layers of partially melted pyroxenite. Pyroxenite layers were separated by a narrow, 2mm layer of chromite. Image analysis on BSE images demonstrate that the median sulphide melt–chromite dihedral angle is extremely low, ~11° compared to ~33° for silicate minerals. These angles are far lower than the percolation threshold (60°) for natural systems. However, low fractions of sulphide melt are trapped within the chromite layer due to the wet grain boundaries. Efficient capillary forces (“sponge” effect) hold the melt in the chromite layer. In contrast, sulphide melt combines within the silicate layer, promoting vertical movement. Additionally, sulphide melt existing above 950°C preferentially leaches Fe^{2+} from chromite causing mss to crystallize. This lowers the S concentration of the melt, lowering Pt solubility which results in the formation of Pt alloys within chromite. The further removal of sulphide melt from chromite layers by re-crystallizing chromites or/and percolation could contribute to extremely high Pt/S within chromites. In conclusion, experimental evidence does indicate that chromites likely acted as a reservoir for evolved Pt-Cu-Ni rich sulphide melts, and that secondary process, including the leaching of Fe^{2+} from chromite caused large amounts of Pt alloys to precipitate in chromitites.

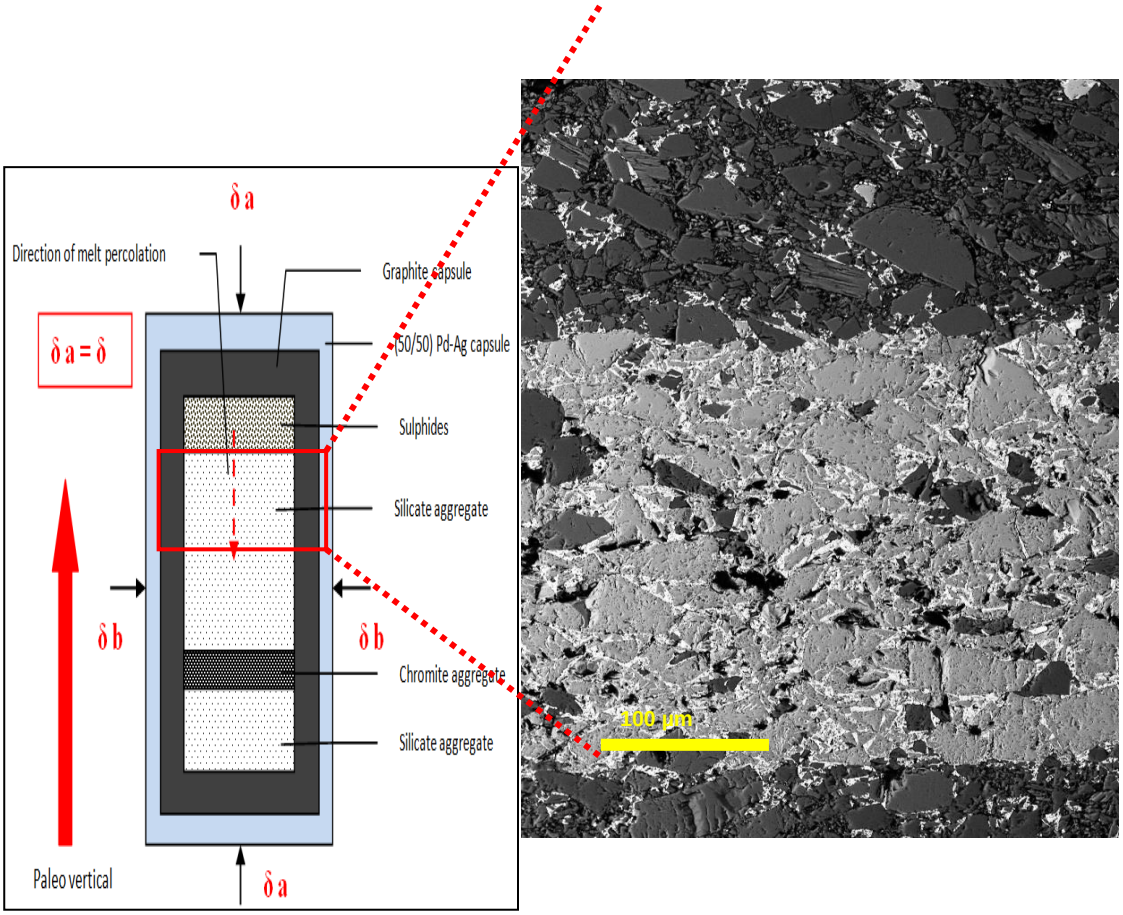

Figure 3: Schematic display of capsule design to imitate sulphide movement through a cumulate pile. The BSE image on the right show a completed experimental run and clearly indicate how sulphides preferentially cumulate in the chromite layers. This figure is assembled from the dissertation of Koegelenberg C., (2011).

Aims

The aim of this investigation is to determine a crystallization sequence in the Fe-Ni-Cu-S system with a composition compatible with the sulphide fraction of the MR. An addition of Pt as trace element to the experimental charge allows for accurate analyses and investigation towards Pt partitioning between the sulphide melt and sulphide solid phase and then the evaluation with the small array of existing experimental data in literature. These criteria could indicate how the sulphide fraction distributed and formed the compositional differentiation in the MR as a function of the stratigraphy. Pt partitioning between the solid and the melt phases would indicate the magnitude of enrichment possible by differentiation of the sulphide system and if this second stage of enrichment of

the sulphide melt could account for the unusual high PGE concentrations associated with the sulphide. This would allow better constrains and some experimental evidence on the magmatic processes leading up to mineralization of the Pt enriched MR and improve our understanding of the processes that shaped the deposit.

Reference list to General introduction

Barnes, S.-J., Maier, W. D., 2002, Platinum-group elements and microstructures of normal Merensky Reef from Impala Platinum Mines, Bushveld Complex: Journal of Petrology, v. 43, p. 103-128.

Campbell, I. H., Naldrett, A. J. & Barnes, S. J., 1983. A model for the origin of the platinum-rich sulfide horizons in the Bushveld and Stillwater Complexes. Journal of Petrology 24, 133-165.

Cawthorn, R.G., 1999a, Platinum-group element mineralization in the Bushveld Complex – a critical reassessment of geochemical models.

Cawthorn, R.G., 1999b, The platinum and palladium resources of the Bushveld Complex: South African Journal of Science, v. 95, p. 481 – 489.

Cawthorn, R. G., Merkle, R. K. and Viljoen, M. J., 2002, Platinum group element deposits in the Bushveld Complex, South Africa. In: Cabri, L. J. (ed.) The Geology, Geochemistry, Mineralogy and Mineral Beneficiation of Platinum-Group Elements. Canadian Institute of Mining and Metallurgy Special Volume 54, p. 389-429.

Cawthorn, R. G., 2005. Pressure fluctuations and formation of the PGE-rich Merensky and chromitite reefs, Bushveld Complex. Mineralium Deposita 40, 231-235.

Eales, H. V. and R. G. Cawthorn, 1996, The BTushveld complex. in Layered intrusions. R. G. Cawthorn, Ed., Elsevier Science B.V.: 181-229.

Godel, B., Barnes, S-J., Maier, W.D., 2006, 3-D Distribution of Sulphide Minerals in the Merensky Reef (Bushveld Complex, South Africa) and the J-M Reef (Stillwater Complex, USA) and their Relationship to Microstructures Using X-Ray Computed Tomography: Journal of Petrology, v. 47, no. 9, p. 1853–1872.

Godel, B., Barnes, S.-J., and Maier, W.D., 2007, Platinum-Group Elements in Sulphide minerals, Platinum-Group Minerals, and Whole-Rocks of the Merensky Reef (Bushveld Complex, South Africa): Implications for the Formation of the Reef: Journal of Petrology, v. 48, no. 8, p. 1569 – 1607.

Kruger, F. J., 1994. The Sr-isotope stratigraphy of the Western Bushveld Complex. South African Journal of Earth Sciences 97, 393-398.

Leeb-du Toit, A., 1986, The Impala Platinum mines. In: Anhaeusser, C. R. & Maske, S. (eds) Mineral Deposits of South Africa. Johannesburg, Geological Society of South Africa, p. 1091-1106.

Li, C. & Ripley, E. M., 2005. Empirical equations to predict the sulfur content of mafic magmas at sulfide saturation and applications to magmatic sulfide deposits. Mineralium Deposita 40, 218-230.

Mavrogenes, J. A. and O'Neill, H. S. C., 1999. The relative effects of pressure, temperature and oxygen fugacity on the solubility of sulphide in mafic magmas. Geochimica et Cosmochimica Acta 63, 1173-1180

Naldrett, A. J., Gasparrini, E. C., Barnes, S. J., von Gruenewaldt, G. and Sharpe, M. R., 1986. The upper critical zone of the Bushveld Complex and a model for the origin of Merensky-type ores. Economic Geology 81(5), 1105-1117.

Naldrett, A. J. & von Gruenewaldt, G., 1989. The association of PGE with chromitite in layered intrusions and ophiolite complexes. Economic Geology 84, 180-187.

Naldrett, A.J., 2004. Magmatic Sulfide Deposits: Geology, Geochemistry and Exploration. Berlin: Springer.

Naldrett, A. J., Wilson, A., Kinnaird, J., and Chunnett, G., 2009, PGE Tenor and Metal Ratios within and below the Merensky Reef, Bushveld Complex: Implications for its Genesis: Journal of Petrology, v. 50, no. 4, p. 625 – 659.

Scoates, J. S., and Friedman, R. M., 2008, Precise age of the platiniferous Merensky Reef, Bushveld Complex, South Africa, by the U-Pb zircon chemical abrasion ID-TIMS technique. Economic Geology v. 103, p. 465-471.

Smith, D. S., Basson, I. J. and Reid, D. L., 2004, Normal reef subfacies of the Merensky

Reef at Northam Platinum Mine, Zwartklip Facies, western Bushveld Complex, South Africa: Canadian Mineralogist v. 42, p. 243-260.

2 Presentation of Paper

PHASE RELATIONS AND Pt SOLUBILITY IN SULPHIDE MELT IN THE FE-NI-CU-S SYSTEM AT 1 ATM: IMPLICATIONS FOR EVOLUTION OF SULPHIDE MAGMA IN THE MERENSKY REEF, BUSHVELD COMPLEX, SOUTH AFRICA.

LUHANN M. THERON, CORNE KOEGELENBERG, GARY STEVENS AND DIRK FREI

Department of Earth Sciences,

University of Stellenbosch, South Africa

2012

***

2.1 Introduction

The Bushveld Complex (BC) is the worlds` largest layered mafic intrusion with an aerial extent of more than 65 000 km2 (Eales & Cawthorn, 1996). The Merensky reef (MR), which is a stratabound platinum (Pt) enriched horizon, was discovered in 1930 by Hans Merensky and extensive mining started in the early 1950s when the demand for platinum-group elements (PGEs) in industrial processes escalated. The BC contains 75% of the world`s Pt resources, which is concentrated in three main stratigraphic units; the Platreef, the UG2 and the MR (Naldrett, et al., 2009). Typically, Pt concentration in the MR varies between 5 – 15 ppm. Thus, as the mafic to ultramafic magmas which formed the complex contain no more than several ppb Pt, it can be concluded that the processes that produced this enrichment in the MR was responsible for a 1000-fold enrichment in Pt (Cawthorn, 1999).

Despite the many years of research, the processes that produced PGE enrichment in the BC reefs are still under debate. Three steps are considered important in forming the MR deposit; 1) magmatic models agree on the importance of sulphide melt as the Pt concentration agent. Pt is able to concentrate in a sulphide melt through the strong partitioning of Pt between sulphide melt and silicate melt (Naldrett & von Gruenewaldt, 1989), 2) repeated injections of new magma batches during the intrusion of the BC can be tracked by changes in mineral assemblage, Mg-number evolution, abrupt changes in isotopic composition and major element composition (Kruger & Marsh, 1982). Pt enriched horizons are considered too often mark the stratigraphic levels within the cumulate pile that record these new magma additions (Cawthorn, 1999) and; 3) bulk sulphide content in the MR only reaches about 6 volume percent but sulphide content peaks in- and just above the thin chromitite seams of the MR (Godel, et al., 2007). Such data suggest that the mineralization processes during

MR genesis was able to enrich specific horizons in PGE by introducing the sulphide fraction in the magma chamber with new magma batch injection episodes and distributing the sulphide as a function of the stratigraphy by movement though a silicate cumulate pile and the prevention of movement by a chromitite pile (Godel, et al., 2007). Although these processes seems elegant and the important role of sulphide magma in concentrating the PGEs are well accepted, the evolution that the sulphide fraction undergone during MR genesis in terms of phase relations with changing temperature and partitioning of major and trace elements, are still poorly constrained.

The problem with studying and interpreting magmatic sulphide processes in nature is that natural samples never preserve their high temperature sulphide mineralogy and the separate sulphide phases we distinguish in natural samples are all the products of re-crystallization and exsolution from a monosulphide solid-solution (MSS) with cooling. This phenomenon in natural samples hampers the study of sulphide fraction behaviour at high temperature conditions. Experimental petrology is the tool that allows for the investigation of sulphide phase relations at high temperature.

The aim of this investigation is to determine a crystallization sequence in the Fe-Ni-Cu-S system with a composition compatible with the sulphide fraction of the MR. An addition of Pt as trace element to the experimental charge allows for accurate analyses and investigation towards Pt partitioning between the sulphide melt and sulphide solid phase and then the evaluation with the small array of existing experimental data in literature. These criteria could indicate how the sulphide fraction distributed and formed the compositional differentiation in the MR as a function of the stratigraphy. Pt partitioning between the solid and the melt phases would indicate the magnitude of enrichment possible by differentiation of the sulphide system. This would allow better

constrains and experimental evidence on the magmatic processes leading up to mineralization of the Pt enriched MR.

2.2 Setting of the Merensky Reef in the BC.

The MR outcrops for ca. 145 km along the western limb of the BC where it is mined extensively. The MR forms the upper most boundary of the critical zone in the Rustenburg Layered Suite. The MR and its stratigraphic setting in the western BC have been described in detail in numerous studies e.g. Leeb-du Toit, (1986); Viljoen, (1999); Barnes & Maier, (2002); Cawthorn, et al., (2002); Smith, et al., (2004); Godel, et al., (2006); and Naldrett, et al., (2008). The MR referred to in this study is normal 'A' type reef (Leeb-du Toit, 1986); (Barnes & Maier, 2002); (Godel, et al., 2006) and (Godel, et al., 2007). This type of MR consists (in an upward paleo vertical direction) of: 1) a medium grained, cumulus, footwall anorthosite (mottled anorthosite in mining terms, ranging in thickness between 1 – 10m). 2) a lower chromitite layer that ranges from 2 to 40mm thick, 3) a varying thickness (0-10m) of coarse grained melanorite (feldspathic pyroxenite in local mining terms); 4) an upper chromitite layer 2-10mm thick with an undulating boundary with the overlain melanorite; 5) an upper 30-225 cm of melanorite.

Sulphide in the MR consist almost exclusively of three intergrowth minerals; pyrrhotite, chalcopyrite and pentlandite in a 40:20:40 ratio and occurs interstitial to cumulus phases of orthopyroxene, plagioclase and chromitite. The highest proportion of sulphide minerals (~6 vol%) occur in the chromitite layers and just above the melanorite and chromitite boundary. Sulphide content decrease moving upwards until the upper chromitite layer. Sulphide content again is high in the upper chromitite and just above the upper chromitite and decreases upwards. See petrographic illustration in Figure 4. (After: Barnes & Maier, 2002).

PGE enrichment occurs on those portions of the stratigraphy that are enriched in sulphide minerals. Godel, et al., (2007), reported that PGE`s (65% - 85%) are not found in solid solution with the base metal sulphides (BMS), but are almost exclusively found as platinum-group mineral (PGM) inclusions in sulphides or located at the contact between BMS and silicates or oxides. Within the MR sulphide composition changes as a function of stratigraphy. Sulphide compositions tend to be more Cu-rich within and just above the chromitite layers and more Fe and Ni dominated upwards (Figure 4). Sulphide minerals in the melanorite layers form networks that are sub-parallel to the paleo vertical and then terminate at the chromitite-silicate interface (Barnes & Maier, 2002).

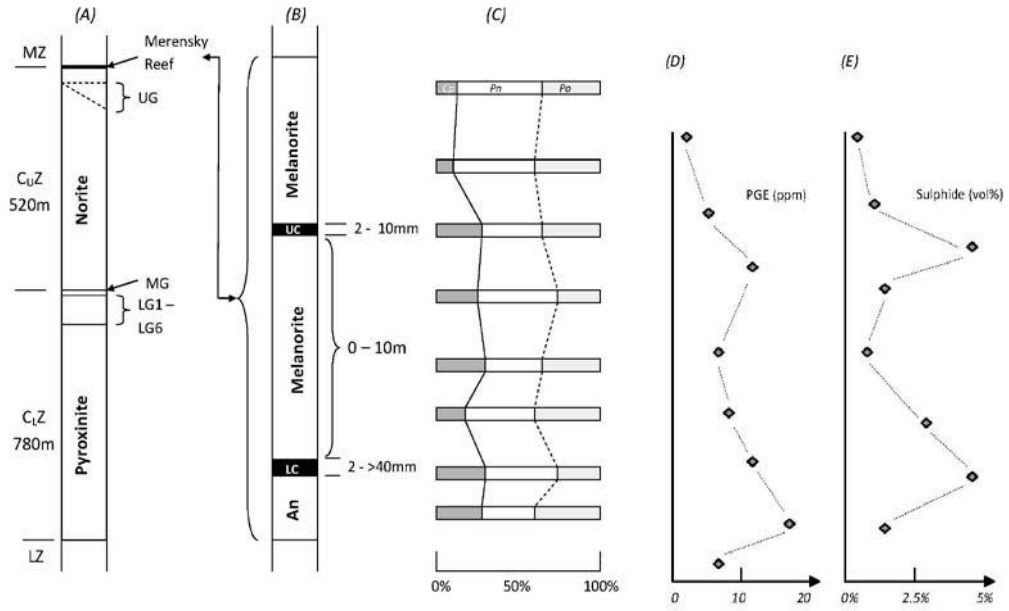

Figure 4: (A) Schematic diagram showing the stratigraphy of the critical zone. (B) Stratigraphy of the MR. (C) Proportions of sulphide minerals as a function of stratigraphy in the MR normalized to 100% sulphide. After Godel, et al., (2007). (D, E) Estimated PGE and sulphide variation as a function of stratigraphy, interpreted from different data sets, including. Naldrett, et al., (2009). Diagrams are not drawn to scale. The heights indicated for the critical zone refer to stratigraphic height within the critical zone in the western BC. In Bushveld literature and mining terminology the melanorite is referred to as pegmatoidal pyroxenite based on the interstitial nature of the plagioclase. As proposed by Barnes & Maier, (2002) this study will use international standard (IUGS) nomenclature for all rocks. Note that, the two chromitite layers are associated with elevated concentrations of PGE and sulphide with peak concentrations just above the chromitites. Abb. LZ – Lower Zone, CLZ – Critical Lower Zone, CUZ – Critical Upper Zone, MZ – Main Zone, UG – Upper

group Chromitites, MG – Middle group Chromitites, LG – Lower Group chromitites, An – Anorthosite, LC – Lower Chromitite, UC – Upper Chromitite, Cp – Chalcopyrite, Pn – Pentlandite, Po – Pyrrhotite.

2.3 Ideas on mineralization processes in the MR

Magmatic processes leading up to PGE enrichment in specific horizons of the BC suggest a few different processes to have occurred. Firstly, the silicate magma which is parent to the BC ore bodies is required to become saturated in sulphur at some point, thereby generating an immiscible sulphide melt (Campbell, et al., 1983). Secondly, strong partitioning of Pt and the other PGEs into the sulphide melt from the silicate melt is required to produce the PGE enriched sulphide melt. As the solubility of PGE in the silicate magma is very low, the sulphide magma needs to interact with a very large volume of silicate magma (Campbell, et al., 1983). Lastly, the sulphide magma movement through the cumulate pile had to physically react differently to the different cumulus phases of oxide and silicate. Therefore the sulphide magma placement within the MR was physically controlled by the sulphide melt and cumulus crystal interaction (Godel, et al., 2006).

The experimental design in this study cannot address the first step which is the point of sulphur saturation and the formation of an immiscible sulphide liquid, but rather the evolution of a sulphide fraction after sulphide saturation. The experimental information on the partitioning of PGEs between a silicate and sulphide melt suggest that it is indeed possible to enrich a sulphide melt extremely efficient through partitioning. Experimental D-values for Pt between silicate and sulphide melt (conc of Pt in sulp. melt/conc. of Pt in sill. melt) are in the order of 104 (Ballhaus & Sylvester, 2000 and Crocket, et al., 1997).

From the compositional distribution of sulphide through the MR stratigraphy (Figure 4) it is evident that the sulphide fraction had undergone significant chemical fractionation. With a fractionating sulphide liquid a secondary partitioning stage for Pt comes to be

important. From a small array of experimental data it is evident that Pt partition between a sulphide solid and sulphide melt phase very strongly. Partition coefficients of Pt between a sulphide solid and sulphide melt phase are in the order of 0.001 and 0.02 (Ballhaus, et al., 2006). This suggests that Pt would re-distribute between a solid sulphide and a sulphide melt phase and the melt would become increasingly enriched in Pt with decreasing temperature. Inaccuracies and untrustworthy calculations of the D-values for trace elements in a sulphide system are often a direct function of the experimental and analytical techniques. More experimental data and more coherent D-values for Pt between sulphide melt and sulphide solid in the compositional range of MR sulphides are needed.

The distribution of sulphide content in the MR is influenced by the physical interaction that a sulphide liquid display towards the oxide and the silicate cumulates (Godel, et al., 2006). Sulphides in the silicate layers of the MR are interconnected in 3 dimensions and fill the interstitial paleovertical dilatencies formed during compaction (Godel, et al., 2006). These dilatencies are proposed to have facilitated downward percolation of the sulphide melt. In the chromitite layers the interconnectivity of the sulphides is negligible and the chromitites acts as a filter preventing further percolation into the footwall of the MR (Godel, et al., 2006). These observations on sulphide mineral distribution are however made on a natural sample of the MR. Remobilization and re-crystallization of the sulphide fraction during the 2 billion year history of the BC is an inevitable reality and the direct interpretation of sulphide melt distribution based on the distribution of sulphide minerals in the rocks could be misleading.

Koegelenberg C., (2011) conducted experimental work which investigated the physical percolation behaviour of the sulphide melt through a silicate-

2chromitite-silicate stratigraphy. This study found that sulphide liquid are extremely mobile through a silicate pile with median dihedral angels between sulphide melt and silicate crystals of 11 º, far below the 60 º threshold for natural geological systems. In silicate layers sulphide melt forms vertical networks promoting the percolation of the melt. In contrast to the silicate layers, chromitite layers show extremely effective wetting properties of the chromite grains by the sulphide melt and hence the chromitite layers serves as a reservoir for the sulphide melt.

2.4 Experimental phase equilibrium in the Fe-Ni-Cu-S system.

The focus of this contribution is to better constrain the chemical fractionation that the sulphide magma undergone during MR genesis. Therefore, describing the fractionation paths of a sulphide system similar in composition to the sulphides of the MR. Much of our understanding of the crystallization sequences in a sulphide magma is derived from the experimental work of Kullerud, et al., (1969), who investigated the ternary systems Fe-Ni-S, Fe-Cu-S and Cu-Ni-S. Since then a number of similar experimental studies have reported rather consistent results on major element partitioning and crystallization sequence in a Fe-Ni-Cu-S system (i.e. Fleet, et al., 1991, Fleet & Pan, 1994 and Barnes, et al., 2001). The relatively good understanding that has been generated by these works can be summarised as follows:

1) Fe-rich MSS is the first solid phase to crystallize from a Cu-Fe-Ni-S melt with metal to sulphur ratios between ~0.8 and ~1.2, indicating partition coefficients for Fe >> 1 (Ballhaus, et al., 2001, Ballhaus, et al., 2006, Godel, et al., 2007, Naldrett, et al., 2009).

2) Cu has a high affinity for the sulphide melt in a Cu-Fe-Ni-S system and this melt will become more Cu-rich during cooling and MSS crystallization. Partition coefficients for Cu are in the order of 0.2

– 0.6. (Fleet & Pan, 1994, Ebel & Naldrett, 1996, Li, et al., 1996). MSS in a Cu-Fe-Ni-S system accommodates more Cu as temperature decreases (Ballhaus, et al., 2001).

3) Ni partitioning is dependent on S fugacity and temperature (Kullerud, et al., 1969, Li, et al., 1996, Ballhaus, et al., 2001). Ni is slightly incompatible with partitioning coefficient around 0.6 at high metal/sulphur ratios of approximately 1.20. In more S-rich systems Ni become more compatible. DNi lies between 0.5 and 2 with a metal/sulphur ratio of 0.9 (Ballhaus, et al., 2001). Ni dissolves as a variety of Ni-sulphides. The Ni1-xS end-member melts just below 1000 °C (Raghaven, 2004c).

4) The compositional variable most influential on the solidus temperature, as noted by Ballhaus, et al., (2001), is metal/sulphur ratio, with higher metal/sulphur ratio depressing the solidus temperature. In a Cu-Fe-Ni-S system with metal/sulphur ratio >1 the solidus is located approximately 150 °C lower than in equivalent systems with metal/sulphur ratio < 1 (Ballhaus, et al., 2006).

2.5 Experimental partitioning of Pt in a sulphide system

The strong partitioning of PGEs from a silicate melt into an immiscible, PGE scavenging sulphide melt is a fundamental characteristic of magmatic mineralization models which seek to explain the PGE-sulphide association in the MR. Consequently, the partitioning behaviour of the PGEs between a silicate- and a sulphide melt have been widely investigated with different sulphide compositions and different Pt concentrations, i.e. Stone, et al., (1990), Crocket, et al., (1997) and Fleet, et al., (1999), also well summarised by Pruseth & Palme, (2004). However, the partitioning of PGEs between a sulphide melt and sulphide solid phase has also significance. Once the sulphide melt has scavenged PGEs from the silicate melt, and it starts to crystallize MSS, the PGEs would partition strongly between these

two phases. Thus, the partitioning of PGEs between the sulphide melt and sulphide solid phase comes to be important when discussing the processes that formed the PGE distribution through the MR.

1. PGE`s partition differently between MSS and sulphide melt. Rh, Ir, and Ru are moderately compatible within MSS whereas Pt and Pd are highly incompatible (Fleet, et al., 1993, Li, et al., 1996, Ballhaus, et al., 2001, Ballhaus, et al., 2006). Typical compatible element D-values are in the order of: Rh~ 3, Ru~ 9 and Ir~ 6.

2. D-values for Pt between MSS and sulphide melt are << 1 and vary as a function of sulphur content. In sulphur under saturated sulphide systems, the sulphur does not occupy all the vacancies in the MSS structure and leaves space for the trace elements, but in sulphur oversaturated systems the S occupies all the vacancies in the MSS and the S content no longer plays a part in the partitioning of the trace elements (Barnes, et al., 2001).Typical D-values for Pt between a sulphide liquid and MSS are between 0.01 and 0.4. (Barnes, et al., 2001, Ballhaus, et al., 2006, Ballhaus, et al., 2001, Fleet, et al., 1993, Li, et al., 1996).

2.6 Experimental details

Starting composition

To ensure that the experimental products are representative of the sulphide fraction of the MR the authors had to produce an experimental starting material which is considered to be a reasonable proxy for the theoretically parent sulphide composition that existed during mineralization of the MR. Lee & Butcher, (1990), after revisiting the Sr-isotope characteristics of the BC, suggested that, even though it seemed unlikely and a drastic action, the sulphides in the MR were introduced by a batch of magma carrying entrained sulphide droplets. (Bockrath, et al., 2004), established through high P-T experiments that the sulphide fraction, in equilibrium with

partially molten upper mantle melts and under mantle P-T conditions, exists in a two phase field with a stable MSS and melt phase. The sulphide melt composition existing in equilibrium with partially molten upper mantle and under mantle P-T condition is: Cu (3.29 at %), Ni (8.95 at %), Fe (36.47 at %) and S (51.29 at %), and this is the composition that would have been entrained in the silicate melt during melt ascent, given that melt ascent is quicker than the settling rate of immiscible sulphide melt from a silicate melt. With calculations considering melt densities, melt proportion and viscosities, (Holzheid, 2012), have unambiguously stated that melt ascent rates are tens of orders of magnitude faster (of all different types of silicate melt) than sulphide settling rates and that sulphide melt would inevitably be washed from the mantle by ascending silicate liquid.

When comparing the theoretical parent sulphide composition as described by Bockrath, et al., (2004) with the average MR sulphide composition, it is noted that the two are very similar (Table 1). Average MR sulphide composition was calculated using the information on sulphide composition and distribution within the MR produced by (Godel, et al., 2007).

Table 1: Comparison of sulphide melt composition in equilibrium with partially molten upper mantle (Bockrath, et al., 2004) and average MR sulphide composition as extracted from Godel, et al., (2007). All concentrations are presented in at%

	Sulphide melt composition in equilibrium with partially molten upper mantle	Average MR Sulphide composition (Adopted from Godel et al, 2007)
Fe (At%)	36.47	34.97
Ni	8.95	11.18
Cu	3.29	4.59
S	51.29	49.27

.

The above mentioned starting material was synthesized from a 99, 9% pure elemental material. $PtCl_2$ was added to the S, Fe, Ni and Cu mixture in an amount that would produce a Pt concentration of 100 ppm. This would ensure that the Pt reacts as a trace element in the system but would likely be present at high enough concentrations in the phases within which it concentrates to ensure easy and accurate analyses by ICP MS. This mixture were hung by a Pd-Ag wire in a vertical tube furnace and heated to 1200 ºC, well above the expected liquidus. The run was allowed to homogenize over night (8 hours) and then detached at high temperature to ensure quenching at that state when it is dropped in cold water. The synthesized material was re-crushed (extra homogenization step) to form the final starting material which is then used in ~5 gram batches for each experimental run.

Experimental P-T conditions

Experiments were performed at 1 atm. conditions. The rationale behind this stems from investigation of phase relations in the sulphide system by Ballhaus, et al., (2006). Experiments in Ballhaus, et al., (2006) were performed at various temperatures and pressures and with various sulphide compositions as starting material. In experiments at 3.0 GPa, the solidus for the system with best compositional correlation to the starting composition in this study (see Table 2), was only 200 °C higher than the equivalent 1 atm solidus. If we consider BC intrusion conditions to be around 0.3 to 0.4 GPa (Scoates & Friedman, 2008)then a solidus change as a consequence of pressure increase from 1 atm. to 0.4 Gpa, would be predicted to be in the range of 25 °C. If we predict that the solidus and liquidus gradients in P-T space are the same for the composition used in this study as in composition S1 of Ballhaus, et al., (2006), then it is expected that the solidus and liquidus would only be ~25 ºC higher. The small variation in solidus and liquidus temperatures in sulphide systems suggest that the results of this well controlled 1 atm. experiments, are generally relevant to melting behaviour of sulphide in the crust.

Table 2: Comparison of the S1 composition used by (Ballhaus, et al., 2006)and the starting composition used in this study. Solidus and liquidus shifts due to pressure may be small, but phase relation details between the composition used in this study and S1 used by Ballhaus, et al., (2006) may differ greatly because of the different S:cation ratios and lower Cu content in S1. All concentrations are given in at%.

	Starting Composition used in this study	S1 (from Ballhaus et al, 2006)
Fe (At%)	36.47	36.03
Ni	8.95	11.65
Cu	3.29	0.37
S	51.29	51.95

Experimental design

Experimental design for the study of partially melting sulphide systems is problematic for several reasons. Melt in a sulphide system undergo quench re-crystallization, meaning that the melt never quench to a homogenous material but rather crystallises to two or more chemically different phases upon quenching. Other aspects that need to be addressed in the design of the experiments are: 1) Oxidation; Experiments need to be conducted in an oxygen free environment to prevent magnetite and SO_2 to form. 2) Volatility; Sulphur becomes a gas at temperatures as low as 60 ºC. The resulting gas pressure can lead to capsule failure if sufficient extra space has not been allowed in the capsule. 3) Porosity; Experimental run products often produce porous experimental products when excess sulphur is not occupied in chemical bonds. This leads to analytical difficulties when measuring the compositions of the run products. During this study we noticed that porosity in the run products is significantly reduced by heating the experimental charge to well above the liquidus and then cooling it to the temperature of the experiment at a rate of ~100 °C/hour.

Experimental design was in principle the same as in many other studies i.e. Ballhaus, et al., (2001), Bockrath, et al.,

(2004), Ballhaus, et al., (2006) and Brenan, et al., (2008). Five grams of the starting material were added to silica glass tube (4mm inner diameter) that had been sealed at one end using an oxygen-acetylene flame. BN was added in a trace amount to act as an oxygen getter. The tubes were then flushed with Ar, evacuated and sealed in the flame. The silica capsules were then hung (in the same way as the synthesis of the starting material) by means of a Pd-Ag wire in a vertical tube furnace. Calibration of the furnace was performed by lowering a thermocouple down the furnace tube. The furnace temperature controller were set at a specific temperature (in this case twice, a lower 900 °C and a higher 1100 °C) and left overnight to stabilize. Then the thermocouple was lowered into the furnace until it read a similar temperature as the furnaces` internal thermometer. This zone is then identified as the Hot-Zone. The specific furnace used in this study, had a Hot-Zone of ~10 cm long. Capsules were heated to 1200 °C, then cooled to the desired equilibrium temperature and kept at constant temperature for between 2 and 15 hours. Experiments were quenched by dropping the capsule into a bucket of cold water ensuring quenching within ±2 seconds. Experiments were performed at 800 °C, 825 °C, 850 °C, 875 °C, 900 °C, 950 °C, 1000 °C, 1025 °C, 1050 °C, 1075 °C and1100 °C.

2.7 Analysis

SEM

The experimental run products were analyzed by means of quantitative ED analysis using a Zeiss Evo MA15VP Scanning Electron Microscope. Polished sections were prepared from the run products and sputter-coated with carbon. Phases were initially identified in backscattered electron (BSE) images, and phase compositions were quantified via EDS analysis using Oxford Instruments® 133KeV detector and Oxford INCA software. Beam conditions during the quantitative analyses were 20KV and approximately 1.5A, with a

working distance of 8.5mm and a specimen beam current of -4.00nA. Energy dispersive spectroscopy is only suitable for determining the concentration of elements present at a level higher that 0.1 wt% for heavy elements, and over 0.2 wt% for light elements. The system is designed to perform high-resolution imaging concurrently with quantitative analyses with errors ranging from ± 0.5 to 0.2 wt% on the major elements. Natural mineral standards of marcasite, pentlandite and cuprite, were used for standardization and verification of the analyses; marcasite for Fe and S, cuprite for Cu and pentlandite for Ni. Analytical uncertainties were determined by analyzing standard materials as unknowns. The relative uncertainties of each element (standard deviation from the published value expressed in percentage.) are: Ni (pentlandite standard) = 0.38; Cu (cuprite standard) = 0.71; S (marcasite standard) = 0.27; and, Fe (marcasite standard) = 0.43.

LA-SF-ICP-MS

Pt concentrations in the run products were determined by LA-SF-ICP-MS using an 213 nm Nd-YAG laser (NewWave UP213) coupled to single collector magnetic sector ICP mass spectrometer (Thermo Finnigan Element 2) at the Central Analytical Facility, Stellenbosch University. The carrier gas into which ablation took place was He. Each sample was analyzed with about 10 laser spots, randomly distributed across the charge. The isotopes recorded were S34, Pt194, and Pt195. All analyses were carried out using a spot size of 55 µm, a repetition rate of 10 Hz and a nominal energy output of 44 %, leading to laser energy of 0.074 J and a fluency of 3.13 J/cm2. The background was collected for 30 s, followed by 60 s ablation and 180 s sample cell washout. All count rates were normalized to S34 in order to correct differences in ablation yield. The average S content of each sulphide phase was previously determined by the SEM ED analytical process described above. An in-house synthesized matrix-matching

standard with a Pt content of 100 ppm was used as the primary calibration material. Data reduction was performed using the GLITTER software package.

2.8 Experimental Results

Phases and textures

Experiments were conducted between 800 ºC and 1100 ºC. The only solid phase to coexist with melt over the whole temperature window was a MSS phase. The highest temperature experiment in which MSS occurred was 1075 ºC, bracketing the liquidus between this temperature and 1100 ºC. The proportion of MSS produced in the run products as a function of temperature is not linear. A temperature decrease of 150 ºC results in crystallization of 75 % of the charge. An additional 150 ºC decrease results in crystallization of only a further 20 % of the charge. MSS crystal size increased systematically with temperature decrease. Largest MSS grains found in the lower temperature run products (around 850 ºC) was ~100 µm in size and smallest MSS grains found in the high temperature run products (around 1050 ºC) was~ 30 µm in size. MSS grain shape is anhedral and crystal boundaries are sharp (see Figure 5F). 120 º Junctions between newly formed crystals is often visible (Figure 5B). MSS grains are homogenously distributed through the experimental run product and show no indication of segregation from the interstitial liquid. Quench crystals of quenched solid solution (QSS) were produced in all experiments above the solidus (Table 3). In the experimental runs above 950 ºC three different types of QSS crystals were produced. These can be seen on the BSE images as having different grey-scale intensities. These are; a Cu-rich phase, a phase with moderate Ni content, and a Ni-rich phase (Table 3A). Below 950 ºC the Ni content in the melt is low enough so that the moderate Ni content QSS crystal does not form and only the high Cu content and high Ni content QSS form (Table 3B). The Ni rich QSS typically crystallizes with a needle-

like shape, with crystals often nucleating on MSS grains. The Cu-rich QSS remains interstitial. These crystals and textures can be seen in the photo template, Figure 5

Major element chemistry

Ten different MSS crystals were analysed in each sub-liquidus experimental run product and both the average and standard deviation calculated. The concentrations of each element in the MSS in Table 4 are given as the average of the ten analyses. The MSS crystals were exceptionally homogenous in composition, as can be seen by the low standard deviation values. Another feature of the MSS was the homogeneity within each crystal. No MSS crystals displayed any detectable zonation. MSS chemistry at each experimental interval is tabulated in Table 4.

QSS phases were analysed individually in the same manner as the MSS (Table 3). Homogeneity was in the same order (Stdev. between 0.5 and 1.0) as the MSS for all the elements. Because of the high resolution possible on the SEM, the possibility of missing a low proportion QSS phase is considered to be low.

The MSS changed composition systematically towards the starting composition, but the composition of the quench phases remained, within error, the same with decreasing temperature. This confirms the interpretation of these crystals as quench products. If they were part of the assemblage that coexisted at equilibrium, it is expected that they would have portrayed a composition trend with changing temperature. Chemistry of the QSS at each temperature interval is tabulated in Table 3.

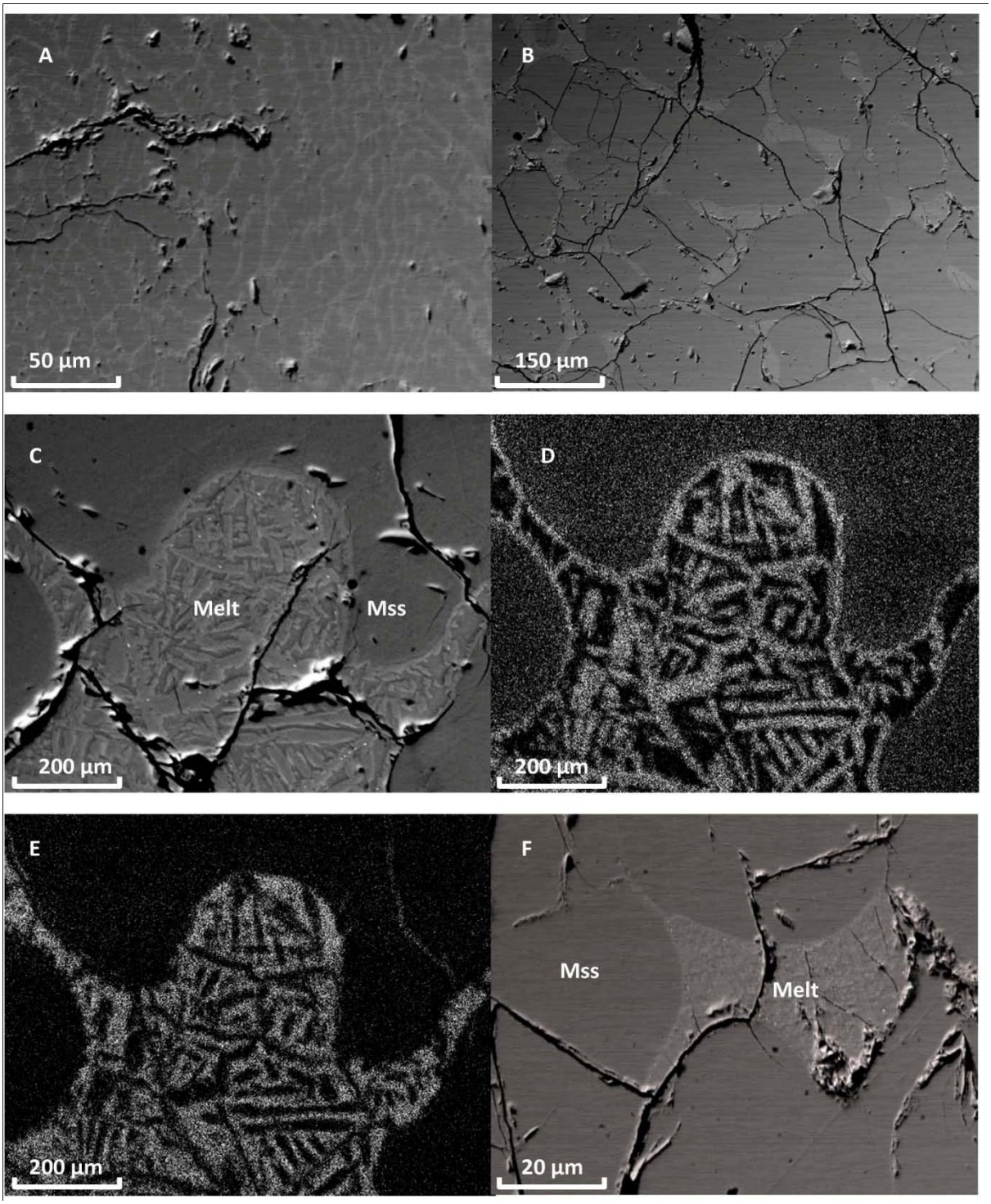

Figure 5: A) SEM BSE image of an experimental run product at super- liquidus conditions showing the quench texture. B) SEM BSE image of an experimental run product equilibrated in the two-phase field (~900 °C) showing MSS and quench textured melt. C) SEM BSE image of the run products at 850 ºC experimental run zoomed into a melt pocket. The image shows the two quench melt products. D) Elemental map of Ni from image C. Ni-rich QSS quenches from the melt in needle like structure and attaches to the MSS crystal boundaries. E) Elemental map of Cu from image C. Cu-rich QSS fills the interstitial space between MSS crystals and Ni-rich quench crystals. F) SEM BSE image from an experiment at 800 ºC showing the smaller isolated melt pocket at lower temperatures close to the solidus.

Calculation of the melt composition

The composition of the melt had to be analysed rigorously. Two possible methods for deriving the equilibrium melt composition were recognised. Firstly by the use of image analyses on the SEM BSE images to determine an accurate MSS/melt ratio, followed by mass balance using the measured MSS and starting mixture compositions to calculate the melt composition. Gray scale image analyses to determine accurate MSS/melt ratios are however challenged due to the fact that the analysis is directly dependant on the quality of the images obtained. In order to obtain clear imagery with well defined grey scale contrasts, the images have to be at a considerably low resolution. This would restrain the analysis to a concentrated area of the run product. The same problem arises when using quantitative area analysis. A third dimension is lost in the run product during the cutting and polishing of the material.

A second method for obtaining the melt composition is by analysing the QSS and MSS phases. As mentioned earlier the QSS phases shows very consistent compositions through the complete temperature range and only changes in proportion to each other. The method of using the QSS compositions and MSS compositions to calculate melt composition involves least square calculations where a solver (programmed in Microsoft excel) is used to manipulate the ratio of QSS to each other and the MSS proportion in the run product, to produce a best fit synthetic composition. This synthetic composition is compared with the known bulk composition. The difference in synthetic composition and known bulk composition is expressed as “r”. With the value of “r” as close as possible to zero, the calculation of the synthetic composition will indicate an accurate estimate of the ratio of QSS to each other. Then using the ratio of QSS and their composition, a melt composition can be calculated. Analysing the QSS increased the resolution of the data considerably because QSS could be

analysed across the complete run product and any heterogeneity could be noticed. Image analyses and mass balance calculations were therefore only used in some experimental run products as a secondary method to support the data obtained by the least square calculations.

I.e. at 900 °C the composition of both the QSS and the MSS are analysed accurately.

- Cu-rich QSS: S = 32.88 wt%, Fe = 34.36 wt%, Ni = 5.92 wt%, Cu = 26,83 wt%

- Ni-rich QSS: S = 33.04 wt%, Fe = 33.33 wt%, Ni = 27.31 wt%, Cu = 6.05 wt%.

- MSS S = 36.98 wt%, Fe = 50.22 wt%, Ni = 9.88 wt%, Cu = 2.91 wt%

Estimated MSS/Melt ratio is: 80:20 (without image analyses).

Table 3: Element chemistry from EDS analyses of the QSS. Three quench phases exists above 950 °C (A) and only two quench phases below 950 °C (B). All the calculations were done with elements concentrations expressed in wt% and only the final melt composition converted to at% (Table 3). “r” is expressed as the error between a calculated synthetic bulk composition and the known bulk composition indicating best fit of the phase proportion estimates. The proportion estimates and the separate QSS compositions were used to calculate the equilibrium melt composition.

A

Exp. Temp.	Quench Phase	S (Wt%)	Fe	Ni	Cu	Phase prop.	
1075	med. Ni	36.54	50.05	11.10	2.31	0.42	
	High Ni	33.60	36.26	25.81	4.33	0.22	
	High Cu	33.31	36.94	3.53	26.22	0.11	
	MSS	37.51	54.46	6.61	1.42	0.25	
Calc. Melt Comp.		35.19	44.02	14.28	6.50	1.00	r = 3
1050	med. Ni	37.38	47.65	12.49	2.48	0.34	
	High Ni	33.89	33.90	26.73	5.48	0.17	
	High Cu	33.42	35.27	4.50	26.81	0.09	
	MSS	38.05	52.56	7.53	1.86	0.40	
Calc. Melt Comp.		35.80	41.91	15.19	7.10	1.00	r = 0.5
1025	med. Ni	36.23	48.20	12.86	2.70	0.25	
	High Ni	32.93	33.41	26.35	7.31	0.19	
	High Cu	32.24	33.85	3.22	30.69	0.07	
	MSS	36.92	52.61	8.21	2.27	0.50	r = 3
Calc. Melt Comp.		34.46	40.77	16.58	8.19	1.00	
1000	med. Ni	36.86	46.19	14.29	2.65	0.10	
	High Ni	33.44	33.49	28.27	4.80	0.17	
	High Cu	32.79	35.75	3.93	27.53	0.08	
	MSS	37.35	51.22	8.74	2.69	0.65	
Calc. Melt Comp.		34.23	37.53	18.72	9.52	1.00	r = 1

B

Exp. Temp.	Quench Phase	S (Wt%)	Fe	Ni	Cu	Phase prop.	
950	High Ni	32.22	32.63	30.47	4.68	0.11	
	High Cu	32.57	35.84	4.48	27.11	0.09	
	MSS	36.64	50.10	10.55	2.71	0.80	r = 3
Calc. Melt Comp.		32.37	34.04	19.05	14.53	1.00	
900	High Ni	33.04	33.33	27.13	6.50	0.13	
	High Cu	32.88	34.36	5.92	26.83	0.05	
	MSS	36.98	50.22	9.88	2.91	0.82	
Calc. Melt Comp.		32.99	33.64	20.75	12.61	1.00	r = 3
875	High Ni	32.62	33.44	30.14	3.80	0.11	
	High Cu	32.52	35.18	2.19	30.10	0.06	
	MSS	36.12	50.19	10.41	3.28	0.83	
Calc. Melt Comp.		32.58	34.04	20.44	12.93	1.00	r = 5
850	High Ni	33.86	35.99	26.85	3.29	0.04	
	High Cu	34.41	37.70	2.19	25.70	0.08	
	MSS	36.74	48.98	11.68	2.59	0.88	
Calc. Melt Comp.		34.21	37.08	11.21	17.50	1.00	r = 4
825	High Ni	33.51	35.73	26.91	3.85	0.05	
	High Cu	33.22	37.08	2.08	27.62	0.07	
	MSS	36.62	49.98	11.32	2.09	0.88	
Calc. Melt Comp.		33.33	36.57	11.54	18.56	1.00	r = 8
800	High Ni	33.13	34.47	27.68	4.72	0.05	
	High Cu	33.08	36.39	2.42	28.11	0.05	
	MSS	36.05	49.77	11.34	2.84	0.90	
Calc. Melt Comp.		33.10	35.50	14.13	17.27	1.00	r = 8

The “synthetic” bulk composition is calculated by using solver to change the QSS ratio. The error is the difference between the synthetic bulk composition and the known bulk composition. The solver changes the QSS ratio so that “r” is as low as possible. The value “r” for each element is squared to make “r” positive. Then the “r” value for each element is summed to produce the total “r” value. In this specific example r = 3. Although this might seem like a high number, it is still considered to be accurate because of the high concentration of some of the elements. For example, sulphur is present in all the melt samples as 35 – 38 wt%. A 1.5 wt% error in the calculations, which is only ~0.5 % inaccuracy, would contribute a value of 2.25 to “r”.

Final melt composition is calculated by using the individual QSS composition and the QSS ratio normalised to 100 %. The equilibrium melt composition at 900 ºC is therefore (converted to at%): S = 47,13 at%, Fe = 27.60 at%, Ni = 16.10 at%, Cu = 9.17 at% (see Table 4).

Table 4: Summary table indicating the final compositions of all the MSS and calculated melts. Concentrations are presented in at% and calculated standard deviation is also expressed in at%. The ± value indicates the analytical error and the standard deviation are calculated from the average values (portrayed as element concentrations in this table) obtained from the ten analyses on each crystal. A) Experimental run conditions showing the temperature, the experimental runtime, the phase analysed and the MSS/melt ratio. B) Major element chemistry as determined by ED analyses. Errors on the analyses of the MSS is a direct function of the analytical error; Ni ± 0.38 at%, Cu ± 0.71 at%, S ± 0.27 at% and Fe ± 0.43 at%. C) Partition Coefficients = Conc. in MSS / Conc. in melt. DCu ranges between 0.19 and 0.27. Stdev) Standard deviation between separate analyses is calculated to show the inter-crystal homogeneity. To keep the Stdev value consistent, all analyses on the MSS were conducted on 10 different crystals. Analyses positions varied on the crystal face, indicating even better MSS homogeneity and complete lack of zonation through single crystals.

A				B								C	
Exp. Temp	Exp. Run (h)	phase	% melt	Atomic % S	STDEV	Atomic % Fe	STDEV	Atomic % Ni	STDEV	Atomic % Cu	STDEV	Metal/ sulfur	D_{Cu}	D_{Ni}
1075	2	MSS		51.31 ± 0.11	0.14	42.77 ± 0.45	0.05	4.94 ± 0.01	0.14	0.98 ± 0.001	0.07	0.95	0.21 ± 0.009	0.45 ± 0.011
		melt	75	49.19 ± 0.21	-	35.32 ± 0.55	-	10.91 ± 0.11	-	4.58 ± 0.101	-	1.03	-	-
1050	5	MSS		51.98 ± 0.11	0.29	41.18 ± 0.44	0.68	5.61 ± 0.01	0.69	1.28 ± 0.001	0.28	0.93	0.26 ± 0.010	0.49 ± 0.011
		melt	60	49.9 ± 0.21	-	33.54 ± 0.54	-	11.57 ± 0.11	-	4.99 ± 0.101	-	1.00	-	-
1025	3	mss		50.74 ± 0.11	0.19	41.52 ± 0.44	0.42	6.16 ± 0.01	0.30	1.57 ± 0.001	0.26	0.97	0.27 ± 0.009	0.48 ± 0.010
		melt	50	48.5 ± 0.21	-	32.94 ± 0.54	-	12.75 ± 0.11	-	5.82 ± 0.101	-	1.06	-	-
1000	4	mss		51.25 ± 0.11	0.14	40.34 ± 0.43	0.27	6.55 ± 0.01	0.24	1.86 ± 0.002	0.19	0.95	0.27 ± 0.008	0.45 ± 0.008
		melt	35	48.35 ± 0.21	-	30.43 ± 0.53	-	14.45 ± 0.11	-	6.78 ± 0.102	-	1.07	-	-
950	5	mss		50.51 ± 0.11	0.17	39.66 ± 0.42	0.21	7.95 ± 0.01	0.14	1.88 ± 0.002	0.14	0.98	0.21 ± 0.005	0.47 ± 0.007
		melt	21	46.37 ± 0.21	-	27.75 ± 0.52	-	17.08 ± 0.11	-	8.79 ± 0.102	-	1.16	-	-
900	5	mss		50.88 ± 0.11	0.15	39.67 ± 0.42	0.21	7.43 ± 0.01	0.18	2.02 ± 0.002	0.20	0.97	0.22 ± 0.004	0.46 ± 0.008
		melt	20	47.13 ± 0.21	-	27.6 ± 0.52	-	16.1 ± 0.11	-	9.17 ± 0.102	-	1.12	-	-
875	12	mss		49.97 ± 0.11	0.16	39.87 ± 0.42	0.21	7.87 ± 0.01	0.15	2.29 ± 0.002	0.30	1.00	0.25 ± 0.005	0.49 ± 0.008
		melt	15	46.66 ± 0.21	-	27.99 ± 0.52	-	16.09 ± 0.11	-	9.25 ± 0.102	-	1.14	-	-
850	4	mss		50.64 ± 0.11	0.33	38.76 ± 0.41	0.56	8.79 ± 0.01	0.36	1.8 ± 0.002	0.60	0.97	0.19 ± 0.004	0.69 ± 0.013
		melt	12	48.29 ± 0.21	-	29.86 ± 0.51	-	12.83 ± 0.11	-	9.03 ± 0.102	-	1.07	-	-
825	7	mss		50.48 ± 0.11	0.14	39.55 ± 0.42	0.22	8.52 ± 0.01	0.19	1.45 ± 0.001	0.27	0.98	0.16 ± 0.003	0.61 ± 0.011
		melt	11	47.53 ± 0.21	-	29.59 ± 0.52	-	13.9 ± 0.11	-	8.97 ± 0.101	-	1.10	-	-
800	6	mss		49.89 ± 0.11	0.20	39.55 ± 0.42	0.49	8.57 ± 0.01	0.20	1.98 ± 0.002	0.63	1.00	0.2 ± 0.004	0.63 ± 0.011
		melt	5	47.27 ± 0.21	-	28.89 ± 0.52	-	13.71 ± 0.11	-	10.14 ± 0.102	-	1.12	-	-

Trace element:

During quenching, not only does the melt quench QSS, but the Pt dissolved in the melt precipitates in a very characteristic way as well. Pt in the run products is concentrated into micro quench crystals (<1 µm in size) which can be easily identified on the BSE images as the bright spots (Figure 6). The Pt partitioned into the MSS is homogeneously dissolved and does not exolve upon quenching. Figure 6 shows these micro crystals to precipitate in close correlation to the Ni-rich quench phase and also to be predominantly concentrated at the boundaries of the MSS grains, where it is likely that the 1st quench crystals would nucleate. Consequently, direct analyses of Pt concentration in the two phase equilibrium experiments were restricted to the MSS crystals, as analysis of the melt domains was rendered unreliable due to inhomogeneous distribution of quench Pt-micro crystals in the quenched melt domains. Pt concentration in the MSS was analysed via LA-SF-ICP-MS. Each analysed experiment (1000 °C, 950 °C, 900 °C, 850 °C, 800 °C) contained 100 ppm Pt in the starting material. Ten randomly chosen MSS. grains in each of the experimental runs were analyzed. Element concentration in Table 5 is given as the average of these 10 analyses. Standard deviation of the Pt concentration in MSS is shown in Table 5 and indicates that MSS is very homogeneous in their Pt content with standard deviation between 0.15 and 1 ppm. Pt concentration in the melts was calculated by mass balance. The errors on the Pt concentration in the melt are therefore inherited from the analytical error on the Pt concentration in the MSS and the estimation error of the MSS/melt ratio.

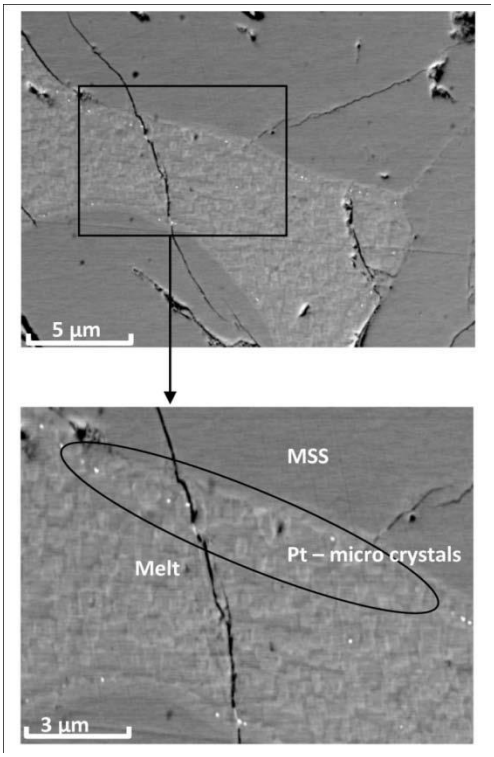

Figure 6: Melt pocket in the two phase field showing how Pt quench crystals form during quenching. Micro crystals form in close correlation, but not exclusively to, with the Ni-rich quenched melt and also to the MSS grain boundaries.

The "r" value obtained in the calculations of the major element melt concentrations is a good indication of the accuracy of the estimated MSS/melt ratio. With the low "r" value obtained in experimental runs 1050 ºC and 1000 ºC indicate that the MSS/melt ratio is possibly very close to accurate. These solutions are however not unique and alternative compositions may exist, although it is deemed highly unlikely. The increasing "r" with the lower temperature experimental runs indicates the increasing inaccuracy of the MSS/melt ratio at low melt proportions. Analytical error on the Pt concentration in the MSS are very low and even with a very conservative error margin for the MSS/melt ratio of 10 %, the error values for the calculated Pt concentration in the melt is still very reasonable (Table 5).

Table 5: Pt analyses of the MSS by LA-SF-ICP-MS. Melt concentrations calculated with mass balance and expressed in ppm. Error in MSS is direct function of analytical procedures and error in melt is error in MSS multiplied by 10 % inaccuracy in MSS/melt ratio. DPt = conc. in MSS/conc. in melt. Calculated Standard deviation is also given in ppm.

Exp. Temp	phase	ppm Pt	STDEV	D_{Pt}
1000	MSS	3.476 ± 0.447	0.175	0.013 ± 0.003
	melt	279.259 ± 0.492	-	-
950	MSS	2.740 ± 0.512	0.147	0.006 ± 0.002
	melt	465.883 ± 0.563	-	-
900	MSS	3.274 ± 0.546	0.474	0.007 ± 0.002
	melt	486.904 ± 0.601	-	-
850	MSS	14.426 ± 3.590	1.131	0.020 ± 0.009
	melt	727.534 ± 3.949	-	-
800	MSS	22.880 ± 1.765	1.012	0.015 ± 0.002
	melt	1565.289 ± 1.942	-	-

2.9 Discussion

Major element evolution of the melt composition with cooling.

In an attempt to understand the role played by sulphide magma evolution during mineralization of the MR, the chemical evolution of melt and MSS with decreasing temperature was investigated. MSS and melt compositions (from Table 4) were plotted on T-X diagrams with X representing element concentration in at% (Figure 7). Systematic changes with temperature in the composition of both MSS and melt can be observed. The trends develop completely as expected from a two phase system where MSS is the only solid phase to equilibrate with the melt. Major element trends are; 1) melt composition approaches the starting bulk composition with increasing temperature; 2) MSS composition approaches the bulk composition with decreasing temperature

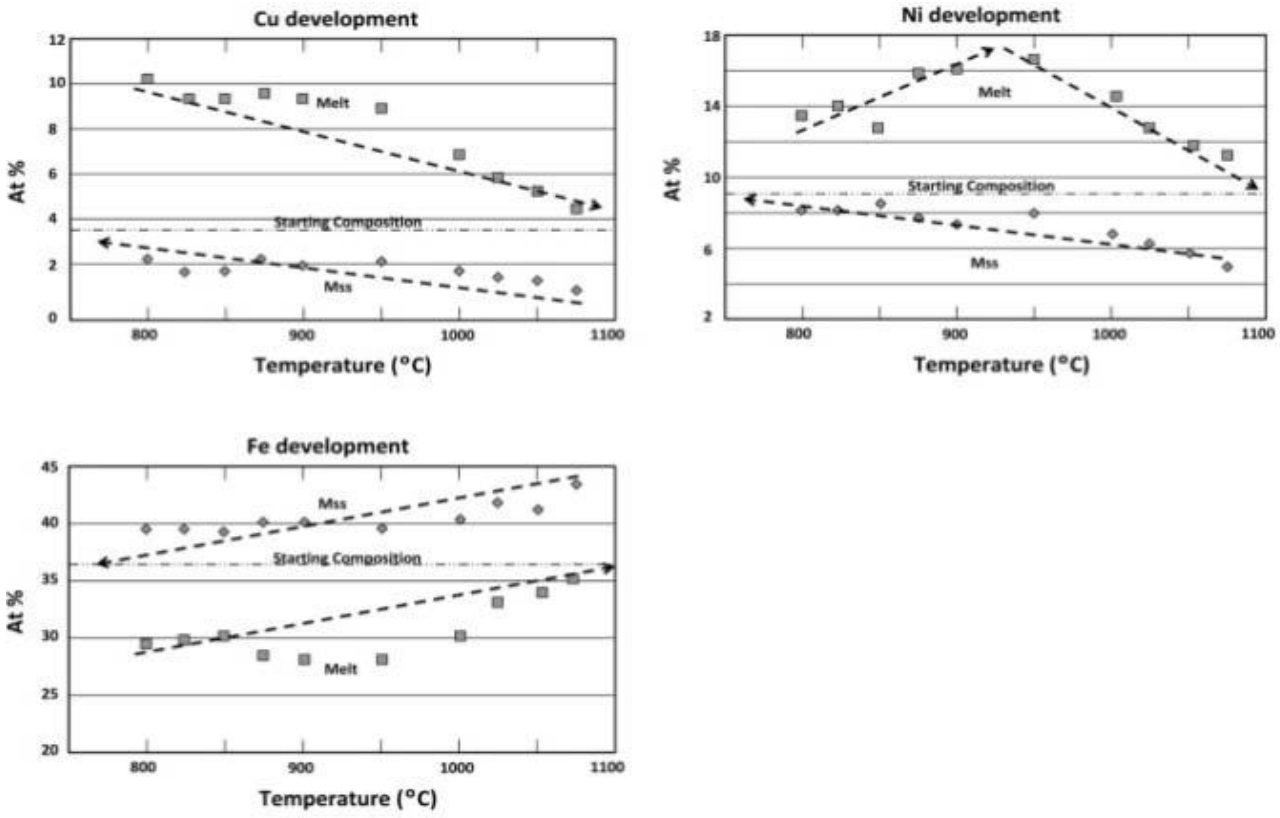

Figure 7: Predictable evolution paths by each element mimicking its partitioning behaviour between the sulphide melt and sulphide solid phases. Arrows indicate the elemental evolution trends with decreasing temperature in the two phase Fe-Ni-Cu-S system.

For all the elements these trends (although not linear) develop in one direction, either increasing or decreasing, but for Ni the slope on the T-X diagram is negative with decreasing temperature from 1200 ºC and positive with still decreasing temperature from 950 ºC. This could be induced by either the influences of sulphur content or by the partitioning behaviour of Ni with changing temperature (Ballhaus, et al., 2001). Sulphur in the melt is fairly consistent (deviates by ~2 at%) over the complete temperature range in this study (see Table 4). The change in partitioning behaviour of Ni between sulphide melt and MSS is therefore considered to be controlled by temperature. At higher temperatures (>875 ºC) Ni partitions preferentially into the melt (DNi varies between 0.45 ± 0.008 and 0.49 ± 0.008) but below 875 ºC Ni partitions into the MSS (DNi lies between 0.61 ± 0.011 and 0.69 ± 0.013). At 950 ºC the system reaches a tipping point for this specific composition. This coincides with the point in the compositional evolution of the melt where Ni content in the melt is low enough for only the two quench phases (high Ni and High Cu) to form during quenching.

Cu partitions preferentially into the melt and DCu varies between 0.16 ±0.003 and 0.27 ± 0.009. Maximum Cu content in the melt of, ~10 at% is reached at very low melt proportions. Cu in solution within MSS increases with decreasing temperature, with Cu content in the MSS approaching ~3 at% near the solidus.

Fe partitions preferentially into MSS, therefore the Fe trend in the melt develops away from the bulk composition with decreasing temperature.

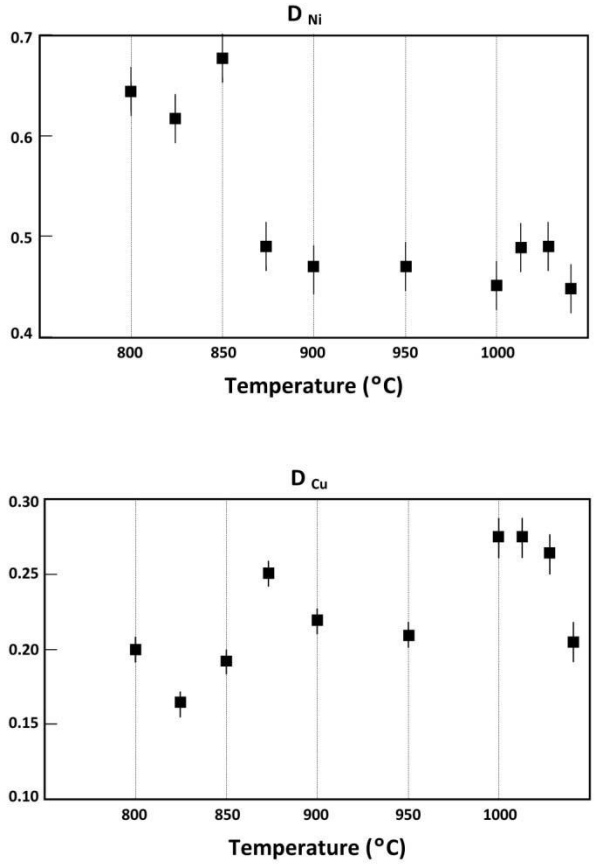

Figure 8: D-values for Cu and Ni with changing temperature. Error margins on D-values are calculated as the difference between the D-values calculated from subtraction of the error on the concentration from the absolute concentration and the addition of the error on the absolute concentration. I.e. at 1000 ºC; the D-value for Cu at 1000 ºC with the concentration of Cu in both the melt and the solid with adding the absolute maximum error to the concentration is: (1.86+0.002)/(6.78+0.102) = 0.27056. And the D-value for Cu at 1000 ºC with by subtraction of the maximum error on both the solid and the melt is: (1.86-0.002)/(6.78-0.102) = 0.27822. Thus the error on the D-value for Cu at 1000 ºC is: 0.27822 – 0.27056 = 0.008.

Partitioning of Pt.

Although D-values of Pt in the literature vary greatly in terms of a minimum and a maximum value (~0.005 to ~0.4) the main control on the partitioning coefficient of Pt between sulphide melt and MSS (as mentioned in the introductory chapters) is bulk sulphur content (Barnes, et al., 2001, Ballhaus, et al., 2006). Accurate LA-SF-ICP-MS analyses on MSS crystals and the known concentration of Pt added to the starting material, allow for accurate calculation of the Pt concentration in the melt in this study (Table 5). The calculated D-values for Pt with changing temperature range between 0.006 ± 0.002 at 950 ºC and 0.02 ± 0.009 at 850 ºC. As mentioned earlier the concentration of sulphur in the bulk composition in this set of experiments was constant. Consequently changes in D-value in this study do not reflect changing sulphur concentration in the system. When compared to studies with similar S-fugacity (Ballhaus, et al., 2001, Ballhaus, et al., 2006 and Barnes, et al., 2001), typically ~50 at% sulphur, the DPt from this study correlates rather well (Figure 9). These experiments were not designed to test the limits of the Pt

solubility in a sulphide melt. However, it can be seen that Pt concentration in the melt exceeds 1.5 wt% at 800 ºC with no Pt-rich phase crystallised in conjunction with MSS in the run products. This is an indication of the extremely high Pt solubility in sulphide melt of this composition.

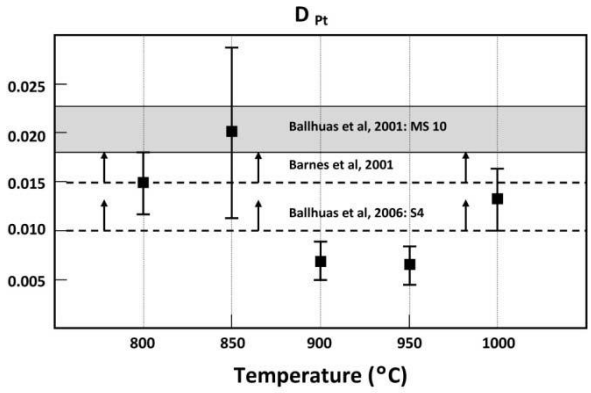

Figure 9: Partition coefficients for Pt with changing temperature. At 900ºC and 950ºC the D-value for Pt in the experimental run product is, within error, lower than found in similar studies. See text for discussion. Error margins in the D-values for Pt were calculated in the same way as for Ni and Cu.

Figure 9 indicates a decrease in D-values for Pt at 900 ºC and 950 ºC and within error these values are lower than those proposed by similar experimental data from other studies. However, the current data base of D-values for Pt between sulphide melt and sulphide solid in similar sulphide composition ranges than this study does not provide enough confidence to conclude that this phenomenon at 900 ºC and 950 ºC is either true or false. But none the less, with such low partition coefficients the sulphide melt of the MR would have been enriched, if compared to bulk starting concentration of Pt, by ~4.5 times (see Table 5). Starting concentration of Pt = 100 ppm, 950 ºC Pt concentration in the melt = 465 ppm).

2.9.1 Fractionation responsible for Sulphide distribution in the MR

As noted in the introductory chapters, sulphide compositions varies with stratigraphic position in the MR. Cu-rich sulphide assemblages are dominant in and just above the chromitite layers and sulphide assemblages become more Fe and Ni dominated and Cu depleted upwards into the hanging wall. The MR consists of two cycles of chromitites followed by a melanorite and both these

cycles are referred to as the MR. For the purposes of this discussion each cycle of chromitite and melanorite shall be referred to as reefs with the melanorite as hanging wall to the chromitite layers. We calculated sulphide composition as a function of the stratigraphy from the extensive geochemical information on sulphide distribution and composition in the MR provided by Godel, et al., (2007). These compositions are plotted together with the MSS and melt compositions produced in this study (Figure 10). The different sulphide compositions plotted are: 1) Average sulphide composition of MR (Table 1). 2) The sulphide composition in the melanorite (hanging wall) and 3) the chromitite (reef) sulphides for each cycle.

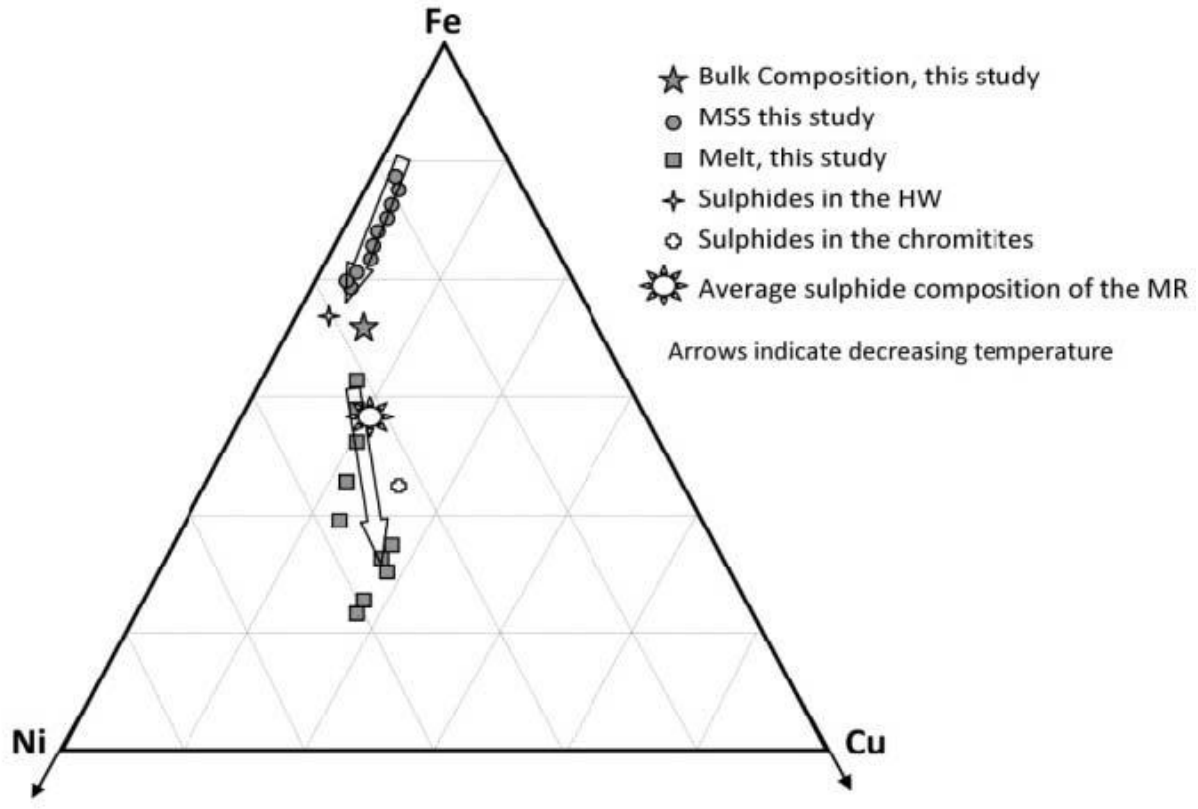

Figure 10: Ternary plot indicating how the average MR sulphide composition indicates a fractionating sulphide liquid. MSS crystals produced as sulphide magma of average MR sulphide composition percolated through the hanging wall, whilst the sulphide in the chromitite represents the melt produced by segregation from these crystals.

From this plot a few key observations can be made:

1) A more Ni and Cu rich composition for the average MR sulphides which closely match with the composition of the 1050 ºC melt, indicates that if the starting composition used in this study is considered a proxy for the parental sulphides to the MR then these sulphides had to undergo fractionation before entering the magma chamber. Alternatively the source for MR sulphide in the mantle could have been more Cu and Ni rich and Fe depleted as the composition thought to exist in equilibrium with partially molten upper mantle as proposed by Bockrath, et al., (2004).

2) The average MR sulphide composition lies between the hanging wall sulphide composition and the chromitite (reef) sulphide composition. The experimental results of this study suggest that the sulphide fraction in the hanging wall represents MSS crystals produced from a sulphide magma of average MR sulphide composition percolated through the hanging wall, whilst the sulphide in the chromitite represents the melt produced by segregation from these crystals.

2.9.2 Fractionation temperature of sulphide liquid

Using the partition coefficients obtained for Cu in this experimental study one can calculate at what melt fraction the sulphide melt represented by the sulphide in the chromitite reefs segregated from the MSS fraction in the hanging wall. This assumes that the descending sulphide melt does not carry any entrained MSS crystals with it. This calculated melt fraction can then be translated into a temperature window using the experimental results from this study. Using the average D-value for Cu from the experiments (0.22), the average Cu concentration in sulphides in the chromitite (7.53 at%), average Cu concentration in the sulphides of the hanging wall (2.49 at%) and the average Cu concentration in MR sulphides (4.59

at%), replaced into a derivative of the Scheil-Gulliver equation, we calculated that the sulphides in the chromitites represent almost 50 % liquid. A 50 % melt fraction indicates 1000 ºC ± 50 ºC. The Scheil-Gulliver derivative for calculating the liquid fraction is as follows:

$$CL = Co(fL)D-1$$

$$(fL)D-1 = CL/Co$$

$$\text{Log } (fL)D-1 = \text{Log } CL/Co$$

$$\text{Log } fL = - \text{Log } CL/Co$$

$$D-1$$

$$fL = 10 \text{ ^ Log } CL/Co$$

$$D-1$$

CL = Concentration in the melt.
Co = bulk concentration.
fL = Liquid fraction.
D = Partition coefficient.

The only way in which this calculation and the parameters used can be reconciled with the mineralization conditions of the MR is to assume that the D-value for Cu is compositionally independent. For if it was not, a different bulk composition to the one we used in this study would indicate different melt proportions and hence a different temperature. When comparing D-values for Cu between a sulphide melt and a sulphide solid from Ballhaus, et al., (2001), it is seen that DCu remains around 0.2 with bulk composition changing in S:cation ratio and total Cu content. We therefore suggests that the less Cu rich bulk composition used in this study and the way it fractionate with decreasing temperature, serves as an accurate proxy for the sulphide fraction found in the MR.

2.9.3 Pt enrichment through fractionation of a sulphide liquid

We have seen that Pt concentrations in normal MR reef often coincide with sulphide peaks. According to the study of Godel, et al., (2007), on the sulphide composition and distribution of normal MR, pentlandite is the most important carrier of PGEs of all the sulphide assemblages, containing 200 – 500 ppm PGE. Pyrrhotite is second riches with 10 – 40 ppm PGE concentrations in 90 % of their analysis and chalcopyrite only

contains 4-10 ppm PGE concentration. If one assumes that all the PGEs is carried within the sulphide fraction of the MR and recalculate PGE content in the sulphide to 100 %, then PGE concentration in the sulphide ranges between 100 ppm and 2500 ppm from the lowest grade portions of the reef to the highest grade chromitite layers of the reef. Using data from Godel, et al., (2007) of Pt concentration in the sulphide fraction of the entire MR, recalculated to 100 % sulphide, average Pt concentration in the sulphide fraction of normal MR would be in the order of 585 ppm Pt. Highest Pt grade in sulphides are however found in the chromitite layers where we suggest the sulphide melt would be trapped.

At ~1000 ºC fractionation temperature (as suggested in the previous section) the partitioning of Pt between a sulphide solid and sulphide melt phase is determined to be around 0.01, This indicates an enrichment factor of 100 times, i.e. at 1000 ºC the melt fraction that separates from the solid fraction would contain 100 times the concentration of Pt. If we calculate the enrichment process backwards from the present Pt grades of sulphides in the chromitite layers, we can determine an estimate of the Pt concentration of the solid sulphide fraction which was left in the hanging wall to the reef during mineralization. If we consider the PGE concentration of the sulphide fraction in the chromitite layers to be around 2500 ppm (Godel, et al., 2007) then the sulphide solid fraction must have contained at least 25 ppm Pt. Godel, et al., (2007) however noted that sulphides immediately above the chromitite layers, which we consider to be the solid fraction, contain ~4 times as much Pt. This could be induced by the way sulphide melt move through the cumulate pile. Sulphide melt will move along vertical networks and once melt volume is too low to retain interconnectivity, droplets of melt (containing higher PGE concentrations) will be trapped (Koegelenberg, 2011).

2.9.4 Sulphide melt movement and trapment in chromitites.

Godel, et al., (2006) recognised that sulphides in the MR are connected in 3-dimensions and proposed that they fill the interstitial spaces and dilatencies that formed during compaction and magma chamber instabilities. The mobility of a sulphide melt through a silicate cumulate pile therefore happened through gravitational percolation via interlinked melt networks. Experiments by Koegelenberg, (2011), used layered experimental charges with silicate and chromitite layers at pressure and measured the dihedral angels between quenched sulphide melts and crystal faces in the different layers. Koegelenberg, (2011) concluded that the average dihedral angel between sulphide melt and silicate crystals is ~33 ° and between sulphide melt and chromite crystals, ~11 °. This is considerably lower than the <60 ° percolation threshold. Consequently, sulphide melt mobility through a silicate and chromitite layers is likely to be effective and rapid. This dihedral angle data however suggests that sulphide melt would form interconnected networks in both silicate and oxide layers of the MR and vertical percolation would be promoted in both layers. Koegelenberg, (2011) suggested that the wetting properties of sulphide melt towards chromitite crystals is very low because of high surface affinity between the two phases. Consequently, capillary forces between the chromitite crystals would create reservoirs of sulphide melt in the chromitite layers. This was clearly demonstrated in the experiments of Koegelenberg, (2011) with sulphide melt moving through a pyroxene + plagioclase layer and being held by a chromitite layer. Additionally, chemical reaction between chromitite crystals and sulphide melt that releases Fe from the chromitites into the sulphide melt was observed to result in precipitation of MSS from the sulphide melt. As a

consequence, the S:cation ratio of the remaining melt is lowered, causing an upwards shift of the solidus and decreasing Pt solubility in the melt. This mechanism is predicted to precipitate Pt within the chromitite layers.

2.10 Conclusion

Pt enrichment and sulphide distribution in the MR is much influenced by the secondary process of sulphide melt differentiation at ~1000 ºC. The differences in composition of the sulphide in the chromitite layers when compared to the sulphide in the melanorite layers correlate well with the melt evolution of the sulphide composition used as experimental starting material. Because of its independence to composition and temperature, Cu were used to calculate the melt fraction at which the sulphides of the MR undergone fractionation and segregation which produced the compositional distribution of sulphide through the stratigraphy of the MR. A 50 % melt fraction was calculated. This 50 % melt fraction was then compared to the MSS/melt ratios found in the experimental run products and indicated a 1000 ºC ± 50 ºC temperature window. At 1000 ºC ± 50 ºC the Cu-rich sulphide melt was able to percolate through the cumulate pile into the chromitite layers where they were trapped by the physical and chemical interaction of chromitite and sulphide melt. The sulphide solid fraction, which is the Fe and Ni dominated MSS, were segregated from the sulphide melt and left behind interspersed with the silicate cumulate crystals of the hanging wall. Pt partitioning between sulphide melt and sulphide solid phases at 1000 ºC are determined to be ~0.01, indicating a 100 times enrichment factor as a secondary process to shaping the MR mineralized horizon. Pt concentrations in the hanging wall to the chromitite layers indicate about 4 times higher concentration. This is suggested to be induced by the physical method of vertically interconnected sulphide melt movement through the silicate cumulate pile.

Reference List

Ballhaus, C., Bockrath, C., Wohlgemuth-Ueberwasser, C. & Berndt, V. L. J., 2006. Fractionation of the noble metals by physical processes.. *Contribution to mineralogy and petrology.,* Volume 152, pp. 667-684.

Ballhaus, C. & Sylvester, P., 2000. Noble Metal Enrichment Processes in the Merensky Reef, Bushveld Complex.. *Journal of Petrology.,* 41(4), p. 545–561.

Ballhaus, C., Tredoux, M. & Spath, A., 2001. Phase relation in the Fe-Ni-Cu-PGE-S system at magmatic temperature and application to massive sulphide ore of the Sudbury Complex.. *Journal of petrology.,* Volume 42, pp. 1911-1926.

Barnes, S.-J. & Maier, W. D., 2002. Platinum-group elements and microstructures of normal Merensky Reef from Impala Platinum Mines, Bushveld Complex.. *Journal of Petrology.,* Volume 43, pp. 103-128.

Barnes, S.-J., van Achterbergh, E., Makovicky, E. & Li, C., 2001. Proton microprobe results for the partitioning of Platinum-group elements between monosulphide solid solution and sulphide liquid.. *South African journal of Geology.,* Volume 104, p. 275 – 286.

Bockrath, C., Ballhaus, C. & Holzheid, A., 2004. Fractionation of the Platinum-Group Elements During Mantle Melting.. *Science,* Volume 305, pp. 1951-1953.

Brenan, J. M., Haider, N. & Andrews, D., 2008. Experimental evaluation of liquid immiscibility in a portion of the system Fe-Ni-Cu-S using high gravitational acceleration.. *Economic Geology.,* Volume 103, p. 1563 – 1570.

Campbell, I. H., Naldrett, A. J. & Barnes, S.-J., 1983. A model for the origin of the platinum-rich sulfide horizons in the Bushveld and Stillwater Complexes.. *Journal of Petrology.,* Volume 24, pp. 133-165.

Cawthorn, R. G., 1999a. Platinum-group element mineralization in the Bushveld Complex – a critical reassessment of geochemical models.. *South African Journal of Science.,* Volume 95, p. 481 – 489.

Cawthorn, R. G., 1999b. The platinum and palladium resources of the Bushveld Complex.. *South African Journal of Science.,* Volume 95, p. 481 – 489.

Cawthorn, R. G., 1999. The platinum and palladium resources of the Bushveld Complex.. *South African Journal of Science.,* Volume 95, p. 481 – 489.

Cawthorn, R. G., 2005. Pressure fluctuations and formation of the PGE-rich Merensky and chromitite reefs, Bushveld Complex.. *Mineralium Deposita.,* Volume 40, pp. 231-235.

Cawthorn, R. G., Merkle, R. K. & Viljoen, M. J., 2002. Platinum group element deposits in the Bushveld Complex, South Africa. The Geology, Geochemistry, Mineralogy and Mineral Beneficiation of Platinum-Group Elements.. *Canadian Institute of Mining and Metallurgy Special Volume.,* Volume 54, pp. 389-429.

Crocket, J. H., Fleet, M. E. & Stone, W. E., 1997. Implications of composition for experimental partitioning of platinum-group elements and gold between sulphide liquid and basaltic melt: the significance of nickel content.. *Geochim. Cosmochim. Acta.,* Volume 61, p. 4139–4149.

Eales, H. V. & Cawthorn, R. G., 1996. *The Bushveld complex. in Layered intrusions.* s.l.:Elsevier Science B.V.: 181-229.

Ebel, D. & Naldrett, A. J., 1996. Fractional crystallization of sulfide ore liquids at high temperature.. *Economic Geology.,* Volume 91, pp. 607-621.

Fleet, M. E., Chryssoulis, S. L., Stone, W. E. & Weisener, C. G., 1993. Partitioning of platinum-group elements and Au in the Fe−Ni−Cu−S system: experiments on the fractional crystallization of sulfide melt.. *Contribution to Mineralogy and Petrology.,* Volume 115, p. 36 – 44.

Fleet, M. E., Crocket, J. H., Liu, M. & Stone, W. E., 1999. Laboratory partitioning of platinum-group elements (PGE) and gold with application to magmatic sulphide-PGE deposits.. *Lithos,* Volume 47, p. 127– 142.

Fleet, M. E., Crocket, J. H. & Stone, W. E., 1991. Partitioning of palladium, iridium and platinum between sulfide liquid and basalt melt: effects of melt composition, concentration and oxygen fugacity.. *Geochim. Cosmochim. Acta,* Volume 55, p. 2545–2554.

Fleet, M. E. & Pan, Y., 1994. Fractional crystallization of anhydrous sulfide liquid in the system Fe-Ni-Cu-S, with application to magmatic sulfide deposits.. *Geochim. Cosmochim. Acta.,* 58(16), pp. 3369-3377.

Godel, B., Barnes, S.-J. & Maier, W. D., 2006. 3-D Distribution of Sulphide Minerals in the Merensky Reef (Bushveld Complex, South Africa) and the J-M Reef (Stillwater Complex, USA) and their Relationship to Microstructures Using X-Ray Computed Tomography.. *Journal of Petrology.,* 47(9), p. 1853–1872.

Godel, B., Barnes, S.-J. & Maier, W. D., 2007. Platinum-Group Elements in Sulphide minerals, Platinum-Group Minerals, and Whole-Rocks of the Merensky Reef (Bushveld Complex, South Africa): Implications for the Formation of the Reef.. *Journal of Petrology.,* 48(8), p. 1569 – 1607.

Holzheid, A., 2012. Seperation of sulfide melt droplets in sulphur saturated silicate liquids.. *Chemical Geology.,* Volume 274, p. 127 – 135.

Koegelenberg, C., 2011. Experimental evidence for Sulphide Melt Percolation and Compositional variation: relevant to the chromitite bearing reefs of the Bushveld Complex.. *Msc. Thesis.*

Kruger, F. J., 1994. The Sr-isotope stratigraphy of the Western Bushveld Complex.. *South African Journal of Earth Sciences.,* Volume 97, pp. 393-398.

Kruger, F. J. & Marsh, J. S., 1982. Significance of Sr87/Sr86 ratios in the Merensky cyclic unit of the Bushveld Complex.. *Nature,* Volume 298, pp. 53-55.

Kullerud, G., Yund, R. A. & Moh, G. H., 1969. Phase relations in the Cu-Fe-S, Cu-Ni-S and Fe-Ni-S systems.. *Economic Geology.,* Volume Monograph 4, pp. 323-343.

Leeb-du Toit, A., 1986. The Impala Platinum mines.. In: *Mineral Deposits of South Africa..* Johannesburg: Geological Society of South Africa., pp. 1091-1106.

Lee, C. A. & Butcher, A. R., 1990. Cyclicity in the Sr isotope stratigraphy through the Merensky and Bastard Reefs, Atok Section, eastern Bushveld Complex.. *Economic Geology,* Volume 85, p. 877–883.

Li, C. et al., 1996. Partitioning of nickel, copper, iridium, rhenium, platinum, and palladium between monosulfide solid solution and sulfide liquid: Effects of composition and temperature.. *Geochim. Cosmochim. Acta.,* 60(7), pp. 1231-1238.

Li, C. & Ripley, E. M., 2005. Empirical equations to predict the sulfur content of mafic magmas at sulfide saturation and applications to magmatic sulfide deposits.. *Mineralium Deposita.,* Volume 40, pp. 218-230.

Mavrogenes, J. A. & O'Neill, H. S. C., 1999. The relative effects of pressure, temperature and oxygen fugacity on the solubility of sulphide in mafic magmas.. *Geochimica et Cosmochimica Acta.,* Volume 63, pp. 1173-1180.

Naldrett, A. J., 2004. *Magmatic Sulfide Deposits..* Berlin: Springer.

Naldrett, A. J. et al., 1986. The upper critical zone of the Bushveld Complex and a model for the origin of Merensky-type ores.. *Economic Geology,* 81(5), pp. 1105-1117.

Naldrett, A. J., Kinnaird, J., Wilson, A. & Chunnett, G., 2008. The concentration of PGE in the Earth's crust with special reference to the Bushveld Complex.. *Earth Science Frontiers.,* 15(5), pp. 264-297.

Naldrett, A. J. & von Gruenewaldt, G., 1989. The association of PGE with chromitite in layered intrusions and ophiolite complexes.. *Economic Geology.,* Volume 84, pp. 180-187.

Naldrett, A. J., Wilson, A., Kinnaird, J. & Chunnett, G., 2009. PGE Tenor and Metal Ratios within and below the Merensky Reef, Bushveld Complex: Implications for its Genesis.. *Journal of Petrology.,* 50(4), p. 625 – 659.

Pruseth, K. L. & Palme, H., 2004. The solubility of Pt in liquid Fe-sulfides.. *Chemical Geology.,* Volume 208, p. 233 – 245.

Raghaven, V., 2004c. Fe-Ni-S (Iron–Nickel-Sulphur).. *Journal of phase equilibria and diffusion.,* Volume 25, p. 373 – 381.

Scoates, J. S. & Friedman, R. M., 2008. Precise age of the platiniferous Merensky Reef, Bushveld Complex, South Africa, by the U-Pb zircon chemical abrasion ID-TIMS technique.. *Economic Geology.,* Volume 103, pp. 465-471.

Scoates, J. S. & Friedman, R. M., 2008. Precise age of the platiniferous Merensky Reef, Bushveld Complex, South Africa, by the U-Pb zircon chemical abrasion ID-TIMS technique.. *Economic Geology.,* Volume 103, pp. 465-471.

Smith, D. S., Basson, I. J. & Reid, D. L., 2004. Normal reef subfacies of the Merensky Reef at Northam Platinum Mine, Zwartklip Facies, western Bushveld Complex, South Africa.. *Canadian Mineralogist.,* Volume 42, pp. 243-260.

Stone, W. E., Crocket, J. H. & Fleet, M. E., 1990. Partitioning of palladium, iridium, platinum and gold between sulphide liquid and basalt melt at 1200 °C.. *Geochim. Cosmochim. Acta.,* Volume 54, p. 2341– 2344.

Tredoux, M., Lindsay, N. M., Davies, G. & McDonald, I., 1995. The fractionation of platinum-group elements in magmatic systems, with the suggestion of a novel causal mechanism.. *South African Journal of Geology.,* Volume 98, pp. 157-167.

Van der Merwe, M. J., 2008. The geology and structure of the Rustenburg Layered Suite in the Potgietersrus/Mokapane area of the Bushveld Complex, South Africa.. *Mineralium Deposita.,* Volume 43, pp. 405-420.

Viljoen, M. J., 1999. The nature and origin of the Merensky Reef of the Western Bushveld Complex based on geological facies and geophysical data.. *South African Journal of Geology.,* Volume 102, pp. 221-239.

Von Gruenewaldt, G., 1973. The main and upper zones of the Bushveld complex in the Roossenekal area Eastern Transvaal.. *Transactions of the Geological Society of South Africa.,* Volume 76, pp. 207-227.

Von Gruenewaldt, G., 1986. Platinum-group element–chromitite associations in the Bushveld Complex.. *Economic Geology.,* Volume 81, p. 1067–1079.